Matthews, L., Przybyłowicz, Ż., Rogers, S. E., Bartlett, P., Johnson, A. J., Sochon, R., & Briscoe, W. H. (2020). The curious case of SDS self-assembly in glycerol: Formation of a lamellar gel. *Journal of Colloid and Interface Science*, *572*, 384-395. https://doi.org/10.1016/j.jcis.2020.03.102

The curious case of SDS self-assembly in glycerol: *Formation of a lamellar gel*

Lauren Matthews[1,2], Żaneta Przybyłowicz[1], Sarah E. Rogers[3], Paul Bartlett[1], Andrew J. Johnson[4], Robert Sochon[4], and Wuge H. Briscoe[1]*

[1] School of Chemistry, University of Bristol, Cantock's Close, Bristol BS8 1TS, UK

[2] Bristol Centre for Functional Nanomaterials, HH Wills Physics Laboratory, University of Bristol, Tyndall Avenue, Bristol BS8 1TL, UK

[3] ISIS Neutron and Muon Source, Rutherford Appleton Laboratory, Harwell Oxford, Didcot, OX11 0QX, UK

[4] GlaxoSmithKline, St George's Avenue, Weybridge, KT13 0DE, UK

*Corresponding author; email: wuge.briscoe@bristol.ac.uk; Tel: +44 (0)117 3318256

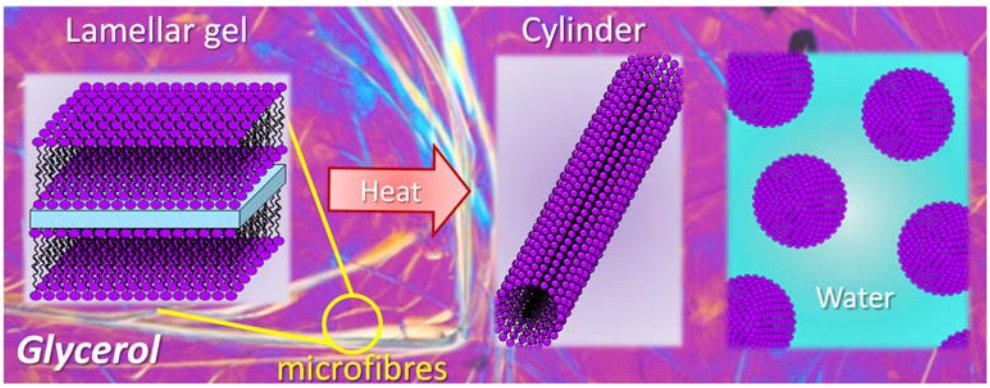

Abstract

Hypothesis – Hydrogen-bonding capacities of polar nonaqueous media significantly affect self-assembly behaviours of surfactants in these media.

Introduction – Glycerol, a nonaqueous hydrogen-bonding solvent, is widely used in industrial formulations due to its desirable physical properties. Surfactants are ubiquitous in such applications; however, surfactant self-assembly in glycerol is not well understood.

Methods – The microscopic structure of the gel phase was studied using a series of imaging techniques: polarised light microscopy (PLM), confocal laser scanning microscopy (CLSM), and environmental scanning electron microscopy (ESEM). The rheological properties of the gel were studied using viscometry and oscillation rheology measurements. Further nano-structural characterisation was carried out using small-angle neutron scattering (SANS).

Results – We have observed the unexpected formation of a microfibrillar gel in SDS and glycerol mixtures at a critical gelation concentration (CGC) as low as ~ 2 wt%; such SDS gelation has not been observed in aqueous systems. The microscopic structure of the gel consisted of microfibres some mm in length and with an average diameter of D ~ 0.5 μm. The fibres in the gel phase exhibited shear-induced alignment in the viscometry measurements, and oscillation tests showed that the gel was viscoelastic, with an elastic-dominated behaviour. Fitting to SANS profiles showed lamellar nano-structures in the gel microfibres at room temperature, transforming into cylindrical-micellar solutions above a critical gelation temperature, T_{CG} ~ 45 ^{o}C.

Conclusions – These unprecedented observations highlight the markedly different self-assembly behaviours in aqueous and nonaqueous H-bonding solvents, which is not currently well understood. Deciphering such self-assembly behaviour is key to furthering our understanding of self-assembly on a fundamental level.

Keywords

Glycerol, Surfactant mesophases, Nonaqueous H-bonding solvents, Gels, Low molecular-weight gels, LMWGs, Small-angle neutron scattering, SANS, Self-assembly, Lamellar gels, Shear thinning

1. Introduction

Understanding surfactant self-assembly in polar nonaqueous solvents is important for industrial applications ranging from shampoos and cosmetics, to paints and coatings. It is also of importance to certain biological processes. For instance, *hyalophoria cecropia* pupae produce a heightened level of glycerol in their blood – conjectured to disrupt water hydrogen-bonding and thus ice formation – to prevent tissue damage in extreme weather conditions during diapause[1-5].

Surfactant/lipid self-assembly in aqueous media is well understood[6-15], with the hydrophobic effect identified as the driving force[16, 17] and the aggregate shape well predicted by the packing parameter[18-21]. At higher surfactant or lipid concentrations, complex mesophases can form and this phase behaviour depends on the amphiphile concentration, pressure, and temperature. However, self-assembly of surfactants in polar H-bonding rich nonaqueous media is less well-understood and it remains unclear if the concepts and theoretical models governing aqueous molecular self-assembly are applicable.

Whilst the interfacial self-assembly behaviour of surfactants in nonaqueous polar media seems to resemble that in aqueous systems, distinct differences in the morphology of the micellar aggregates have been reported in solution, with micellar phases observed in low concentration surfactant mixtures[22] and more complex phases or hydrated crystals in higher concentration mixtures[23, 24]. For instance, in ethylene glycol, nonionic octaethylene glycol monotetradecyl ether ($C_{14}E_8$) formed elongated rod-like micelles and ionic sodium dodecyl sulfate (SDS) or dodecyltrimethylammonium bromide (C_{12}TAB) formed ellipsoidal micelles[25, 26]. $C_{10}E_4OMe$ ($C_{10}H_{21}O(C_2H_4O)_4CH_3$) was found to have a critical micelle concentration (CMC) of 11.6 mM and form a monolayer at the air-water interface[27, 28].

In glycerol specifically, Khan *et al.*[22] showed that the Krafft point, T_K, of SDS increased from ~ 16 ^oC in pure water to 31 ^oC in pure glycerol. The CMC in the glycerol/water mixture, assessed using the pendant drop method, was found to increase with the amount of glycerol (*i.e.* from 8.1 mM in water to *vs* ~ 35 mM in glycerol), pointing different self-assembly behaviours.

Here, we report an unusual self-assembly behaviour of sodium dodecyl sulfate (SDS) in glycerol. The well-established aqueous mesophase diagram[8, 9] shows that SDS would form spherical or ellipsoidal micelles at a CMC of 8.1 mM[29], and then a lamellar phase at ~80 wt%. In contrast, we have observed that SDS formed a gel at a concentration as low as 2.3 wt%. The structure of this complex gel phase was probed microscopically with polarising light microscopy (PLM), confocal laser scanning microscopy (CLSM), and environmental scanning electron microscopy (ESEM). Further structural information was obtained from small-angle neutron scattering (SANS) and rheological measurements. The observation of this unexpected gel phase, not formed at such low SDS concentrations in aqueous media, highlights the complexity of self-assembly behaviour of surfactants in H-bonding nonaqueous media which is not currently fully understood.

2. Materials and Methods

2.1 Materials

h-Sodium dodecyl sulfate (SDS) (Sigma-Aldrich, > 98.0 %) was recrystallised three times from ethanol prior to use, and its purity was monitored with ^{1}H NMR. *h*-Glycerol (Fisher Scientific, > 98.0 %) and *d*-Glycerol (Sigma-Aldrich, > 98.0 % and > 98.0 atom % D) were used as received. All glycerol-containing (both *hydrogenated* (*h*-) and *deuterated (d*-)) phases and controls were kept sealed from moisture. Nile red (Sigma-Aldrich), a hydrophobic dye, was dispersed in *h*-glycerol and then added to the gel phases for confocal microscopy imaging. The gel-like phase was prepared by adding *h*-SDS to *h*- or *d*-glycerol, then incubating the mixture in a shaker incubator (Stuart SI505) for two hours at 60 ^{o}C whilst it was shaken at 550 RPM, before equilibrating at room temperature overnight.

2.2 Surface tensiometry

Equilibrium surface tension was carried out in ambient conditions using a Krüss K100 tensiometer using the Wilhelmy plate method, using an inert platinum plate, which was cleaned by flaming between measurements. Due to the viscosity of *h*-glycerol, the samples were left to equilibrate for 30 minutes to allow for diffusion of surfactant to the air-liquid interface.

2.3 Polarised light microscopy (PLM)

PLM was carried out using a Nikon Eclipse E200 microscope, where the polarisers were crossed at 90^{o} with respect to each other and images were captured using the PixeLINK® Capture OEM software with a 530 nm first-order waveplate inserted in the optical patch. PLM measurements were carried out under ambient conditions, using a 40 x magnification.

2.4 Confocal laser scanning microscopy (CLSM)

CLSM was carried out using a multi-laser confocal scanning laser microscope (Leica SP5), where an Argon laser (λ_{ex} = 488 nm) was used to excite the dye added to the gel phase (Nile red). The lens used in the imaging was a 63 x magnification glycerol lens, as the match in the refractive index with the solvent allowed for better image quality.

2.5 Environmental scanning electron microscopy (ESEM)

ESEM was carried out using a scanning electron microscope (Quanta 200 – FEI FEG-SEM) operating at a low vacuum to image the 'wet' phase, and a solid-state detector to collect backscattered electrons. The phase was found to be conductive, and thus, coating was not necessary for imaging.

2.6 Viscometry and oscillation rheology

All rheological measurements were performed using a rotational rheometer (Malvern Panalytical Kinexus Pro) in a cone-plate geometry (CP 4/20), due to the wall-depletion effect observed in oscillation measurements[30]. Viscometry measurements were carried out with the shear rate decreasing from 100 s^{-1} to 0.001 s^{-1} and each measurement was run for three minutes or until it reached a steady state equilibrium. Oscillation measurements involved first characterising the linear viscoelastic region while changing the deformation applied, at a constant frequency of 1 Hz. A strain value was then selected from this linear region for frequency sweep measurements.

2.7 Small-angle neutron scattering (SANS)

SANS data was obtained from samples contained in quartz cells with a 2 mm path length over 0.5 h integration time on the LOQ[31, 32] or Sans2d[33, 34] small-angle diffractometer at the ISIS Pulsed Neutron Source (STFC Rutherford Appleton Laboratory, Didcot, UK). LOQ utilizes neutrons with wavelengths λ = 2 – 10 Å and the data was collected in the $\boldsymbol{q}$ range of 0.008–1.6 $Å^{-1}$. For Sans2d, a $\boldsymbol{q}$-range of 0.002 – 0.5 $Å^{-1}$ was achieved utilizing neutrons of λ = 1.75 – 10.75 Å. The raw scattering data was corrected for the detector efficiency, sample transmission, and background scattering and converted to scattering cross-section data ($\partial\Sigma/\partial\Omega$ *vs* $\boldsymbol{q}$) using MantidPlot[31, 35, 36]. The data was then converted to an absolute scale (cm^{-1}) using the scattering intensity from a standard sample (a solid blend of hydrogenous and perdeuterated polystyrene) in accordance with established procedures[37].

2.8 SANS data analysis

The SANS data at 25 ^{o}C was fitted using the lamellar phase models in SasView. The general scattering intensity for lamellar systems is described as[38, 39]

$$I(\boldsymbol{q}) = \frac{2\pi VP(\boldsymbol{q})S(\boldsymbol{q})}{d\boldsymbol{q}^2} \qquad (\mathbf{1})$$

where V is the scattering volume; $P(\boldsymbol{q})$ is the form factor that describes the shape of the particles or the phase present; $S(\boldsymbol{q})$ is the structure factor that describes the interparticle interaction; and d is the lamellar spacing.

Of the five lamellar models in SasView [38-41], we used a lamellar stack paracrystal model, in which individual lamellae stacks in solution were independent of each other, with the SDS layer considered as a whole rather than separated into a headgroup and a tail layer.

The SANS data at 70 °C was fitted using a cylindrical form factor and a Hayter-MSA structure factor in SasView. The general scattering intensity for cylindrical systems is described as[42, 43]

$$P(\boldsymbol{q},\alpha) = \frac{F^2(\boldsymbol{q},\alpha)\sin(\alpha)}{V} \quad (\mathbf{2})$$

where

$$F(\boldsymbol{q},\alpha) = 2(\Delta\rho)V\frac{\sin\left(\frac{1}{2}\boldsymbol{q}L\cos(\alpha)\right)}{\frac{1}{2}\boldsymbol{q}L\cos(\alpha)}\frac{J_1(\boldsymbol{q}R\sin\alpha)}{\boldsymbol{q}R\sin\alpha} \quad (\mathbf{3})$$

and α is the angle between the cylinder axis and $\boldsymbol{q}$; $\Delta\rho$ is the contrast in scattering length density; V is the cylinder volume; L is the cylinder length; R is the cylinder radius; and J_1 is the first order Bessel function.

3. Results and Discussion

3.1 Surface tensiometry of SDS in glycerol

The surface tension, γ, *vs* $\ln(c_{SDS})$, plots in both glycerol and water are shown in **Figure 1**, with the CMC, minimum surface tension γ_{min}, and the headgroup area A_{HG} at ~CMC determined from the measurements listed in **Table 1**. The tensiometry data indicates surface activity of SDS in glycerol at the room temperature, with surfactant adsorption to the air-glycerol interface as γ decreased with c_{SDS} to a critical point - the CMC, after which it became constant with increasing c_{SDS}, analogous to the aqueous system.

The CMC value of SDS in glycerol is higher than that in water (11.7 *vs* 8.1 mM), likely due to a stronger solvophobic effect in water than in glycerol, consistent with a higher surface tension (and thus a higher cohesive energy) of water (72.8 mN m^{-1}; cf. **Table 1**) compared to that of glycerol (64.0 mN m^{-1}). This is also consistent with a lower minimum surface tension at the air-

water interface (γ_{min} = 38.3 mN m^{-1})[44] compared to that at the air-glycerol interface (γ_{min} = 46.0 mN m^{-1}). Lastly, the optimal headgroup area, A_{HG}, can be determined through calculation of the surface excess $\Gamma = -(d\gamma/d\ln(c_{SDS}))/2RT$ in the linear region in the γ-ln(c_{SDS}) plot preceding the CMC. As shown in **Table 1**, SDS had a similar optimal headgroup area A_{HG} = 46.0 Å^2 at the air-glycerol interface than that at the air-water interface (A_{HG} = 43.5 Å^2)[44].

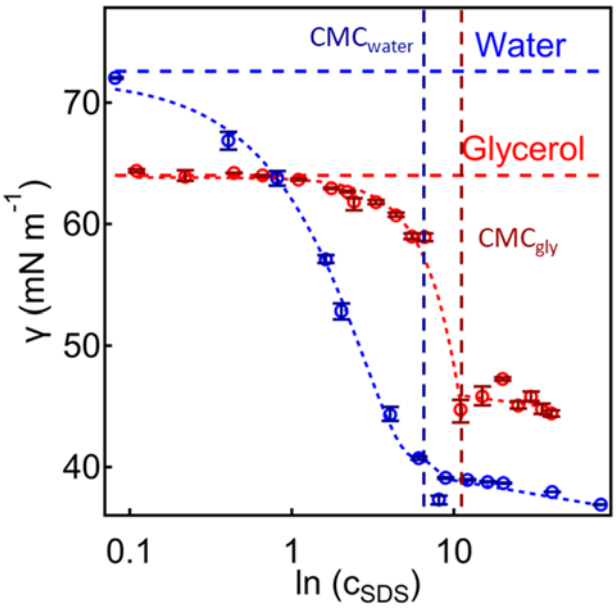

Figure 1 Surface tension, γ, *vs* ln(c_{SDS}), for SDS at the air-glycerol (red circles) and air-water (blue circles) interface at room temperature. The surface tensions of the pure solvents are indicated by the horizontal dashed lines.

Table 1 A summary of the surface tension parameters determined from surface tensiometry measurements of SDS in water and glycerol: the surface tension of the pure solvent (γ_0), the minimum surface tension after addition of SDS (γ_{min}), the critical micelle concentration (CMC), the surface excess (Γ), and the surfactant headgroup area (A_{HG}).

Solvent	γ_0 (mN m^{-1})	γ_{min} (mN m^{-1})	CMC (mM)	Γ (10^{-6} mol m^{-2})	A_{HG} (Å^2)
Water	72.8	38.3	8.1	3.82	43.5
Glycerol	64.0	46.0	11.7	1.66	46.0

3.2 The formation of a low molecular-weight gel (LMWG)

SDS was added to glycerol at a concentration range of 0.2 – 4.4 wt% (or 10 – 220 mM); as the surface tension data above shows a CMC of 0.3 wt% (or 11.7 mM) SDS in glycerol, this corresponded to an SDS concentration of ~ 0.6 – 14.7 CMC. All the samples appeared

transparent and fluid at 60 °C (**Figure 2a**). Upon cooling to room temperature (25 °C), an opaque gel-like phase was observed in the samples with SDS concentration > ~2.3 wt% (~7.7 CMC), which could hold its own weight upon inversion (**Figure 2b**). For comparison, a transparent liquid phase was retained throughout the SDS concentration range in aqueous media (not shown), unable to hold its own weight upon inversion, consistent with an aqueous globular-micelle solution[8, 9].

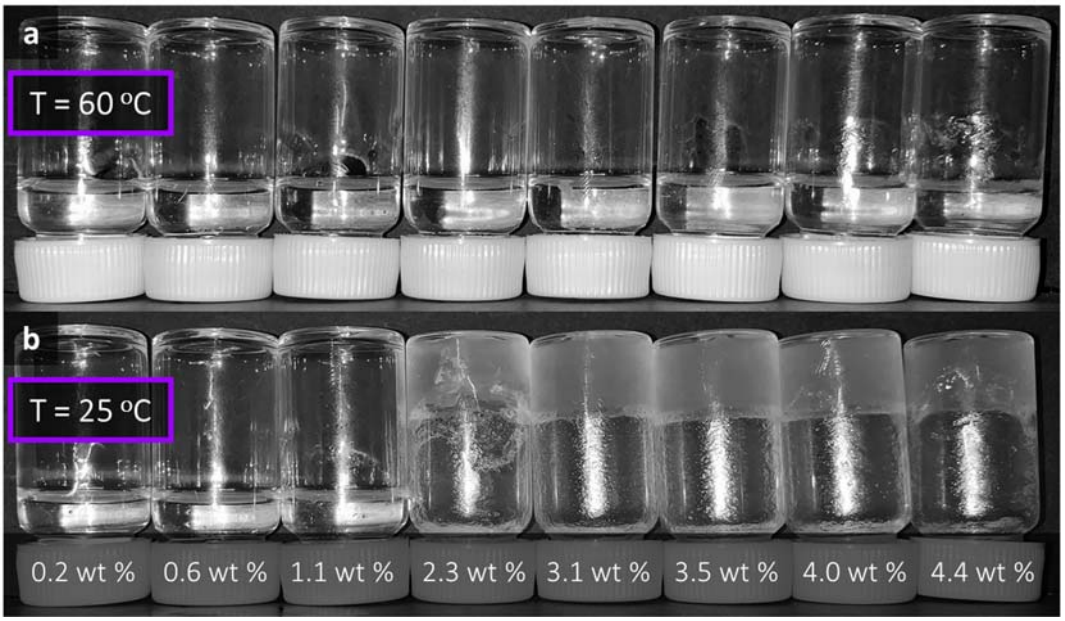

Figure 2 (**a**) Inverted glass vials containing ~3 mL of transparent liquid SDS micellar solution in glycerol with different concentrations of SDS (labels in **b**) immediately after they were heated at 60 °C and shaken at 550 RPM for 2 h. (**b**) After being left overnight at room temperature, the samples with > 2.3 wt% (~7.7 CMC) SDS formed an opaque gel-like phase.

Meanwhile, even at SDS concentration as low as 0.8 wt% (3.7 CMC), fibrillar aggregates were observed (visible by eye) (**Figure 3**), pointing to the elongated aggregate structure, which could be responsible for the gelation. Entangled fibrillar aggregates are well known to be present in low molecular-weight gels (LMWGs) arising from elongated wormlike aggregates[45-48]. However, such fibrillar aggregates structures with SDS concentrations as low as 2.3 wt% with no other additives have not been reported previously in glycerol media.

The effect of temperature on the formation of the phase is also exemplified in **Figure 2**, with the gel-phase "melting" at elevated temperatures, conjectured to arise from the breakup of the fibrous aggregates to form SDS globular micelles, similar to those observed in aqueous systems.

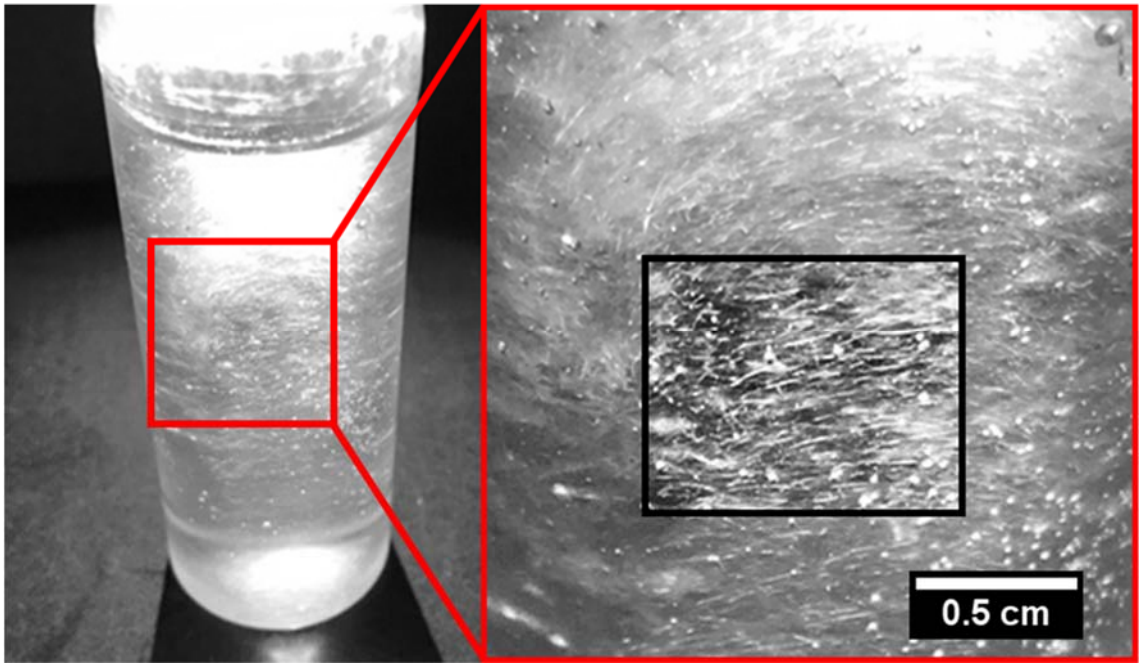

Figure 3 Photographs of the fibrous aggregates present in a glycerol solution with ~ 0.8 wt% SDS, with a magnified fibre-rich region (**Right**) showing that the fibre length was on the order of mm. (**Right**, **inset**) A section of the image highlights the fibre morphology and size with an enhanced contrast.

3.3 Microscopic structure of gel-like surfactant mesophase

Polarised light microscopy (PLM) showed the presence of an anisotropic phase (**Figure 4a** and **b**), consisting of entangled fibrillar aggregates with no long-range ordering. The length of these fibres could not be probed with this technique, as the fibres were longer, on average, than the field of view. The fibre morphology was either straight (**Figure 4a**) or curved (**Figure 4b**), indicative of flexible fibrillar aggregates.

The fibrillar aggregates are reminiscent of elongated wormlike aggregates, often resulting in gel-like material properties[49, 50] and usually with the addition of a co-surfactant[51-54] or salt[55-58]. Wormlike micellar solutions are an example of low molecular-weight gels (LMWGs) and, aside from their wormlike appearance, they have characteristic rheological responses to shearing[59-63]. Such gels arise from physical entanglement (as opposed to chemical crosslinking) of wormlike micelles, making them readily deformable. Wormlike micelles aspect have useful for applications such as drug delivery[64, 65], as their cylindrical shape allows for high cellular uptake[66, 67].

Although the fibre length is not accurately accessible here, the fibre diameters were found to be up to 20 µm (not shown) and highly polydisperse. This diameter is two orders of magnitude larger than the typical SDS wormlike micelle diameter of ~35 - 41 Å in aqueous salt solutions[68-72], pointing to the hierarchical nature of the microfibres. The structure of the fibres was confirmed in environmental scanning-electron microscopy (ESEM, Figure 4c and d).

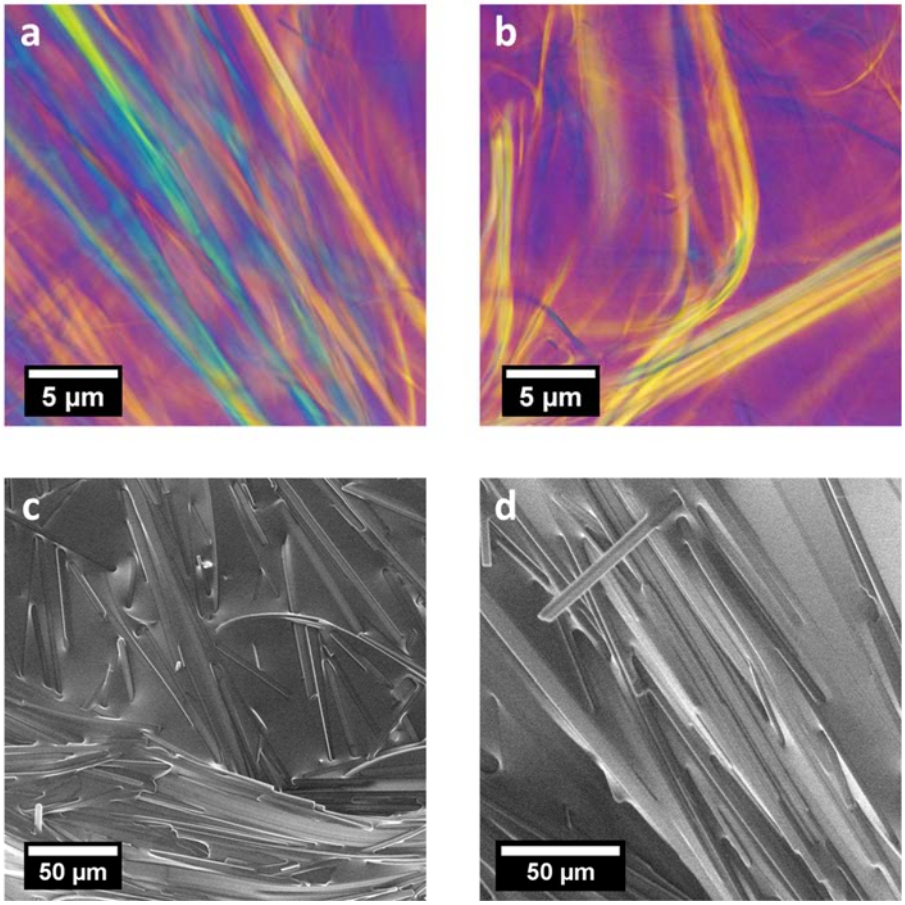

Figure 4 (a, b) PLM images and (c, d) ESEM images of the fibrillar aggregates present in 4.4 wt% SDS in glycerol.

Furthermore, confocal microscopy was facilitated by adding a hydrophobic dye (Nile red, λ_{ex} = 488 nm) to tag the hydrophobic parts of the fibres (Figure 5a). The high contrast between the fibres and glycerol allowed determination of a statistical distribution of the fibre diameter *D*, with a peak value at ~0.49-0.50 µm in a range of 0.1 – 1.4 µm (Figure 5b). The average fibre diameter was D_a ~ 494 nm, two orders of magnitude larger than that of an SDS wormlike micelle in aqueous solution[68-72]. This again confirms that the fibrillar aggregates could not be composed of single SDS wormlike micelles and that the microfibres were of hierarchical structure.

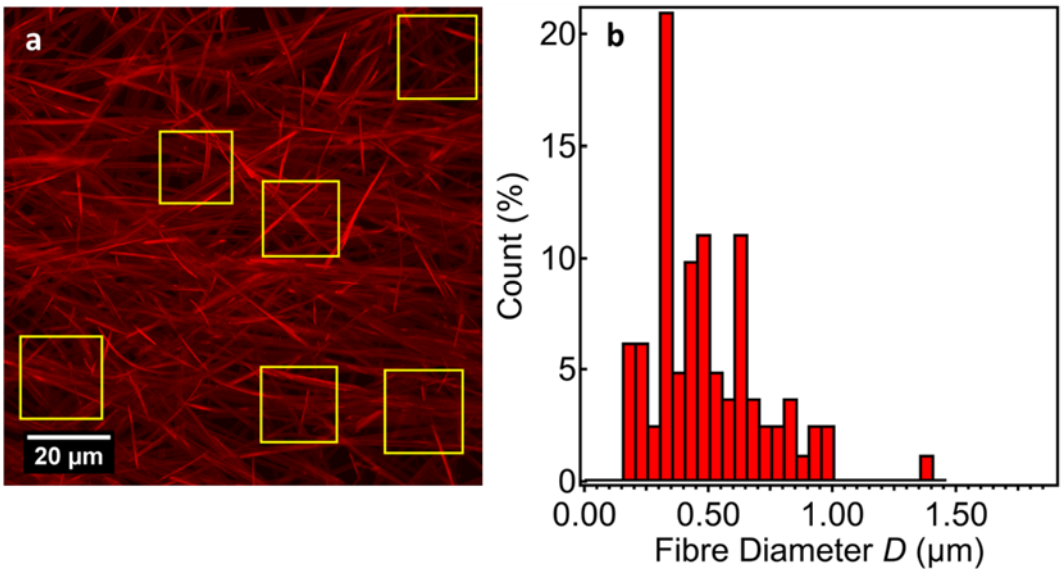

Figure 5 (**a**) Confocal micrograph of the microfibrillar structure in the 4.4 wt% SDS-in-glycerol gel. The yellow boxes indicate the regions in which the fibre diameters were measured, with its distribution shown in (**b**).

Thus, the microscopy observations confirm that the microscopic structure of the gel network consisted of fibrillar aggregates. The low SDS concentrations at which the gelation occurred in the absence of other additives suggest that self-assembly in glycerol is very different from that in water.

3.4 Rheological properties of the LMW SDS-in-glycerol gel

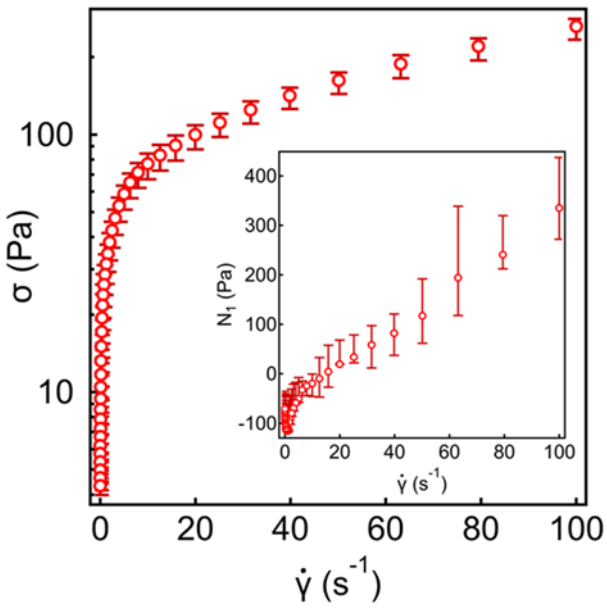

Figure 6 Shear stress, σ, *vs* shear rate, $\dot{\gamma}$, for the SDS-in-glycerol gel (4.4 wt%; ~14.7 CMC). The inflection point in the curve is indicative of shear thinning non-Newtonian fluid behaviour (with

possible fibre breakage). (inset) Corresponding first normal stress difference, N_1, *vs* shear rate, $\dot{\gamma}$, with the log-log plot shown in Figure S1 in SM.

The shear stress magnitude sustained by the gel (σ < 250 Pa) over the shear rate $\dot{\gamma}$ range investigated (Figure 6) is consistent with a weak physical gel. Figure 6 also shows shear thinning behaviour with a non-linear shear stress-shear rate (σ-$\dot{\gamma}$) relationship, which is not characteristic of ideal Newtonian fluids. The presence of an inflection point in the σ-$\dot{\gamma}$ plot indicates shear alignment within the gel, commonly observed in polymer melts[73-77] and wormlike micelle solutions[59, 60, 63, 78-80], consistent with the microfibrillar aggregate structure observed in the gel. Breakage of the microfibres could also occur upon shear along with shear-induced alignment, and further structural characterisation using *in situ* rheo-SANS and post-shear PLM could help to shed lights on such structural transformations.

The first normal stress difference N_1 over the $\dot{\gamma}$ range is shown in the inset (Figure 6, with the log-log plot shown in Figure S1 in SM), which is the difference (and thus the anisotropy) between the stress value in the shear direction and that in the direction perpendicular to shear. The plot shows a general increase in N_1 with $\dot{\gamma}$, from an initial negative value to large positive values, indicating increased structural anisotropy due to shear attributable to the fibrous aggregates becoming elongated in the direction of the applied shear, again consistent with a microfibrillar structure.

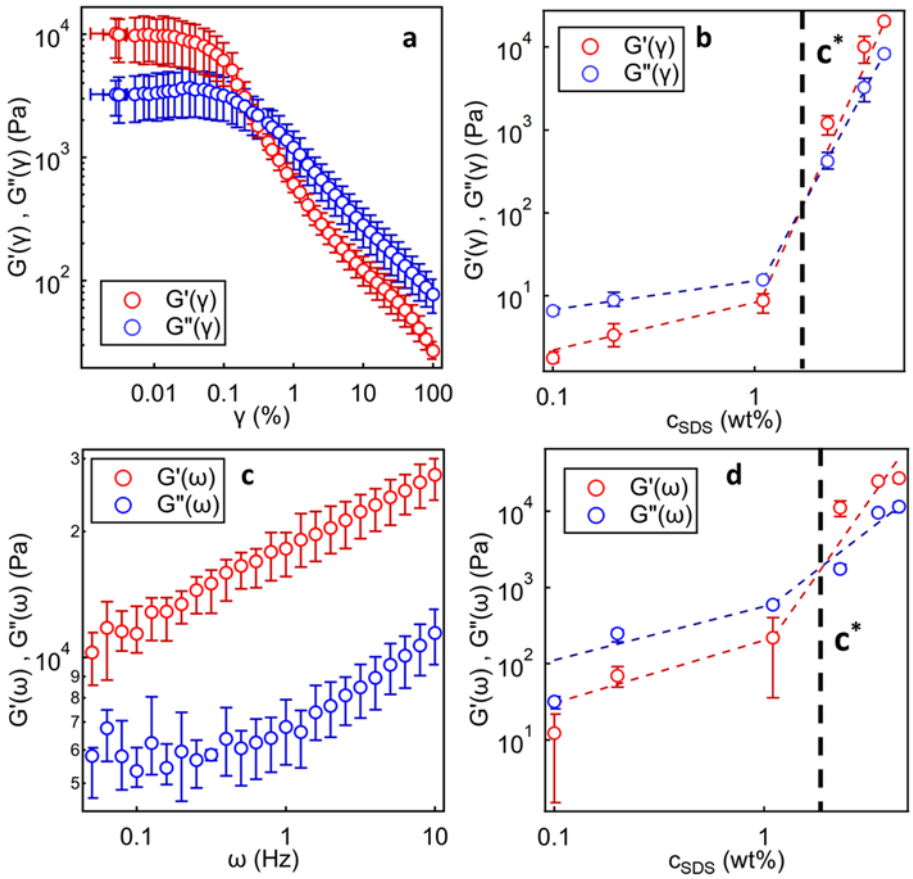

Figure 7 (**a**) *G*' (elastic, red) and *G*" (viscous, blue) as a function of shear strain, *γ*, for the gel (4.4 wt% SDS; ~14.7 CMC), with an initial plateau linear viscoelastic region (LVER). (**b**) The variation of *G*' and *G*" with the SDS concentration, c_{SDS}, at *γ* = 0.001 %. (**c**) *G*' (elastic, red) and *G*" (viscous, blue) as a function of the frequency, *ω*, for the gel (4.4 wt% SDS). (**d**) The variation of *G*' and *G*" with the c_{SDS}, at *ω* = 10 Hz.

Table 2 Values for the slopes in the liquid and gel regimes of the plots of the elastic (*G*') and viscous (*G*") moduli *vs* c_{SDS} for the amplitude (*γ* = 0.001 %) and frequency (*ω* = 10 Hz) sweep measurements in Figure 7(b) and (d), respectively.

Modulus	Regime	Modulus *vs.* c_{SDS} Slope (Pa)
G'(γ)	Liquid	0.146
	Gel	116.0
G"(γ)	Liquid	0.197
	Gel	48.9
G'(ω)	Liquid	189.4
	Gel	8678.6
G" (ω)	Liquid	489.9

Gel	3642.2

The elastic and storage moduli (G' and G'', respectively) are plotted as a function of strain (γ), to illustrate the viscoelastic behaviour of the gel, as shown in **Figure 7a**. An initial linear viscoelastic region (LVER) indicates that the structure of the system (as commonly observed in all materials) was unaffected by small deformations. Given the strength of this gel, it is also tempting to compare with the stronger gels formed by semiflexible networks, such as actin filaments or microtubules. The MacKintosh model[81] describes a relation between G' and the bending modulus, κ, where $G' \sim \kappa^2$. The estimated κ values using this model are plotted against c_{SDS} in **Figure 8**, giving $\kappa \sim 140$ Pa for the microfibrillar aggregates constituting the gel at the highest c_{SDS} investigated. In comparison, actin filaments[82] exhibited a bending modulus $\kappa \sim$ pPa, much lower than that observed here; whereas gelatin fibres[83] exhibited $\kappa \sim$ kPa, closer to the values observed here.

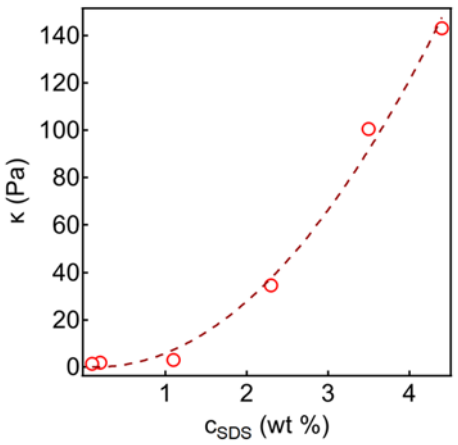

Figure 8 The bending modulus, κ, as a function of c_{SDS} with a guideline showing the non-linear relation. κ was determined using the MacKintosh model[81] and the plateau G' values from amplitude sweep measurements.

Beyond the LVER, both G' and G'' decreased by two orders of magnitude, indicating that the fibrillar structure was sensitive to larger deformations. It is possible that the elongated structures were broken into smaller aggregates, leaving globular aggregates at high shear deformations. The gel appeared elastic at low deformations with $G' > G''$; however, as the deformation was increased, the viscous modulus, G'', became dominant, arising from the presence of globular aggregates, making the phase more liquid-like.

The plateau value of the two moduli at a low deformation (γ = 0.001 %) are shown in **Figure 7b** as a function of SDS concentration, c_{SDS}. Whilst at higher SDS concentrations, the gel exhibited a predominantly elastic behaviour, the viscous modulus G'' dominated at lower SDS concentrations. This is also consistent with the physical appearance of the system: at low c_{SDS}, it appeared as a transparent liquid that was able to flow. These shear measurements confirm a fluid to gel transition occurring between 1.1 – 2.5 wt% (~3.7 – 8.3 CMC) SDS - consistent with the macroscopic visual observation in Fig. 3; the concentration for this transition can be defined as a **critical gelation concentration, *CGC***.

Figure 7c shows that both G' and G'' increased with the frequency, ω, with the gel exhibiting largely elastic behaviour (i.e. $G' > G''$ with no cross-over) over the frequency range investigated. The moduli, however, seemed less sensitive to the frequency compared to the strain, suggesting that the gel was more sensitive to the deformation applied, as opposed to the speed at which it was applied (**Figure 7a**). However, the convergence of the moduli at lower frequencies could be indicative of the presence of viscoelastic fibrillar networks[84], where the relaxation time is slower than the one measurable with the experimental technique.

The magnitude of the moduli (G' ~ 27 kPa and G'' ~ 11 kPa, respectively, at ω = 10 Hz) is relatively high for the SDS-in-glycerol gel (c_{SDS} = 4.4 wt%). This compares with the literature moduli values for surfactant-based gels[80, 85-89], typically from elongated wormlike aggregates, in the range of 10 – 100 Pa, although with some exceptions up to G' = ~ 8 kPa[90]. This indicates that the SDS-in-glycerol gel was both highly viscous and highly elastic. It is also tempting to compare this with the stronger gels formed by semiflexible biopolymer networks, such as actin filaments or microtubules

Figure 7d shows the variation in the moduli with c_{SDS} at high frequency (ω = ~10 Hz), which follows a similar trend to that in **Figure 7b**, where there is a crossover from a viscous fluid to an elastic gel in the range c^* = 1.1 - 2.5 wt%. This points to an entangled fibrillar network at higher c_{SDS} and liquid-like globular micelle solutions at lower c_{SDS}.

3.5 Gel nanostructure from SANS

SANS measurements revealed a lamellar mesophase in the gel evident from the emergence of the equally spaced Bragg peaks at $\boldsymbol{q}$ = 0.11, 0.22, and 0.34 Å^{-1} (indicated by the vertical dashed lines in the figure), attributed to n_α = 1, 2, and 3 lamellar peak order, as c_{SDS} approached ~2.3

wt% (**Figure 9**). The Bragg peaks were more pronounced at c_{SDS} = 4.4 wt% that at lower SDS concentrations (cf. **Figure 9** for c_{SDS} = 2.3 wt%). The lamellar *d*-spacing calculated from the Bragg peak positions is *d* ~ 57 Å, larger than that reported in aqueous systems (*d* ~ 38 Å[8, 9]) and indicating *h*-SDS bilayers swollen with inter-bilayer glycerol.

Figure 9 also shows the distinctive transition in the SANS profile at c_{SDS} = 1.1 wt% (~3.7 CMC) SDS concentration, where there was no low-***q*** turnover comparable to the SANS profile of the gel sample at higher c_{SDS}; the Bragg peaks were also absent, indicating that, at low SDS concentrations, the lamellar structure was not present.

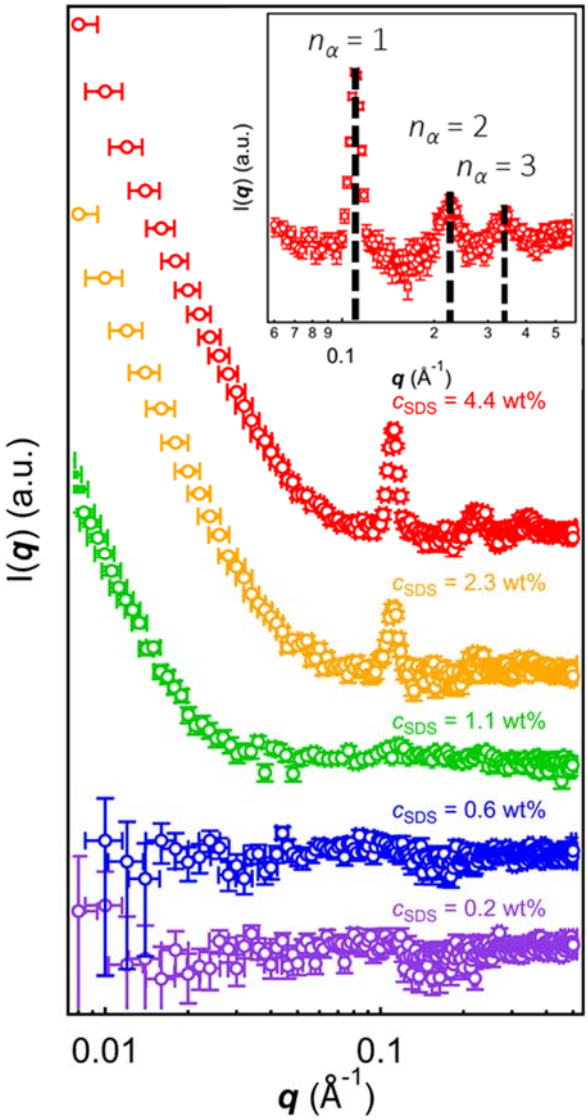

Figure 9 SANS profiles for *h*-SDS in *d*-glycerol at various surfactant concentrations c_{SDS} at room temperature. Enlarged view of the Bragg peaks for 4.4 wt% shown in the **inset**. The profiles are offset on the vertical scale for clarity.

The effect of temperature on the SANS profile for the *h*-SDS-in-*d*-glycerol gel (C_{SDS} = 4.4 wt%) is shown **Figure 10**. The transition from the lamellar phase to a micellar phase is distinctive in the SANS profile, occurring between T = 40 and 50 °C, which we term as the *critical gelation temperature (CGT)*. The micellar phase shows the presence of a structure factor, indicative of interactions between micellar aggregates in solution, which has been observed in aqueous ionic surfactant solutions[91].

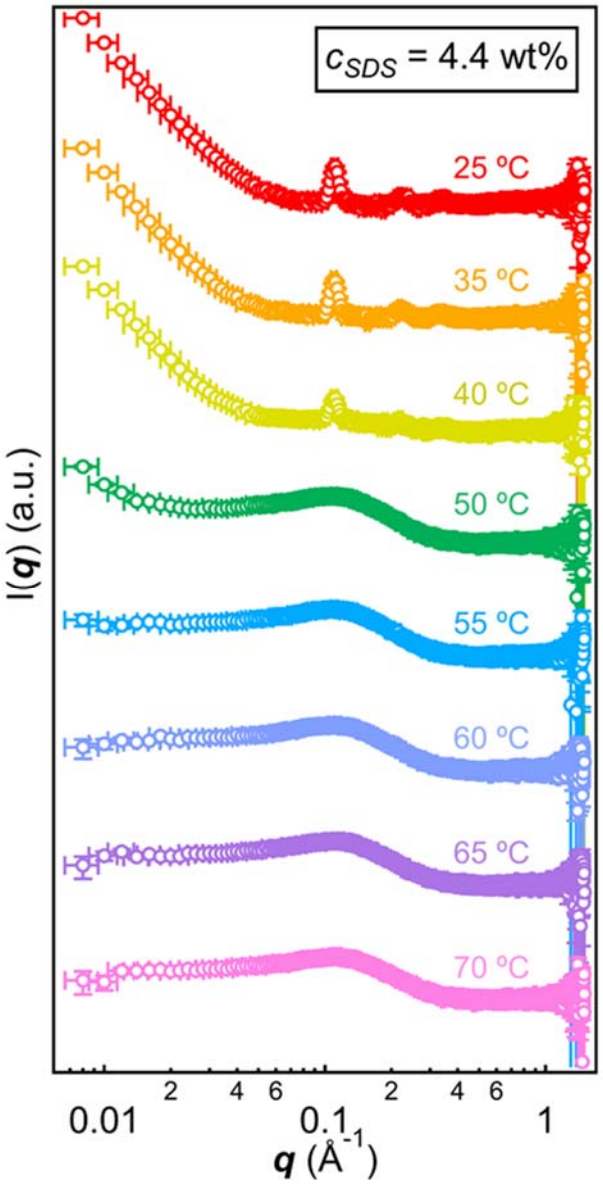

Figure 10 SANS profiles for 4.4 wt% (~14.7 CMC) *h*-SDS in *d*-glycerol at different temperatures, showing the transition between the micellar solution to the lamellar phase at a critical gelation temperature CGT ~ 40 – 50 °C.

Of five different lamellar models trialled, the paracrystal lamellar stack model was found to best fit the gel SANS profiles. **Figure 11a** shows an example fit to the 4.4 wt% (~14.7 CMC) *h*-

SDS in *d*-glycerol gel, with the corresponding fitting parameters including the χ^2 value listed in **Table 3**. This model describes multiple lamellar stacks in solution, oriented anisotropically with respect to each other (**Figure 11c**).

The analysis here shows that the thickness of the *h*-SDS bilayer to be t_L = 48.1 Å, whereas the lamellar *d*-spacing is *d* = 55.6 Å. Therefore, the structure of the lamellar phase must incorporate a layer of intercalating *d*-glycerol molecules (Δd ~ 8 Å, corresponding to 1.5-2 glycerol molecule widths) that solvate the SDS headgroups.

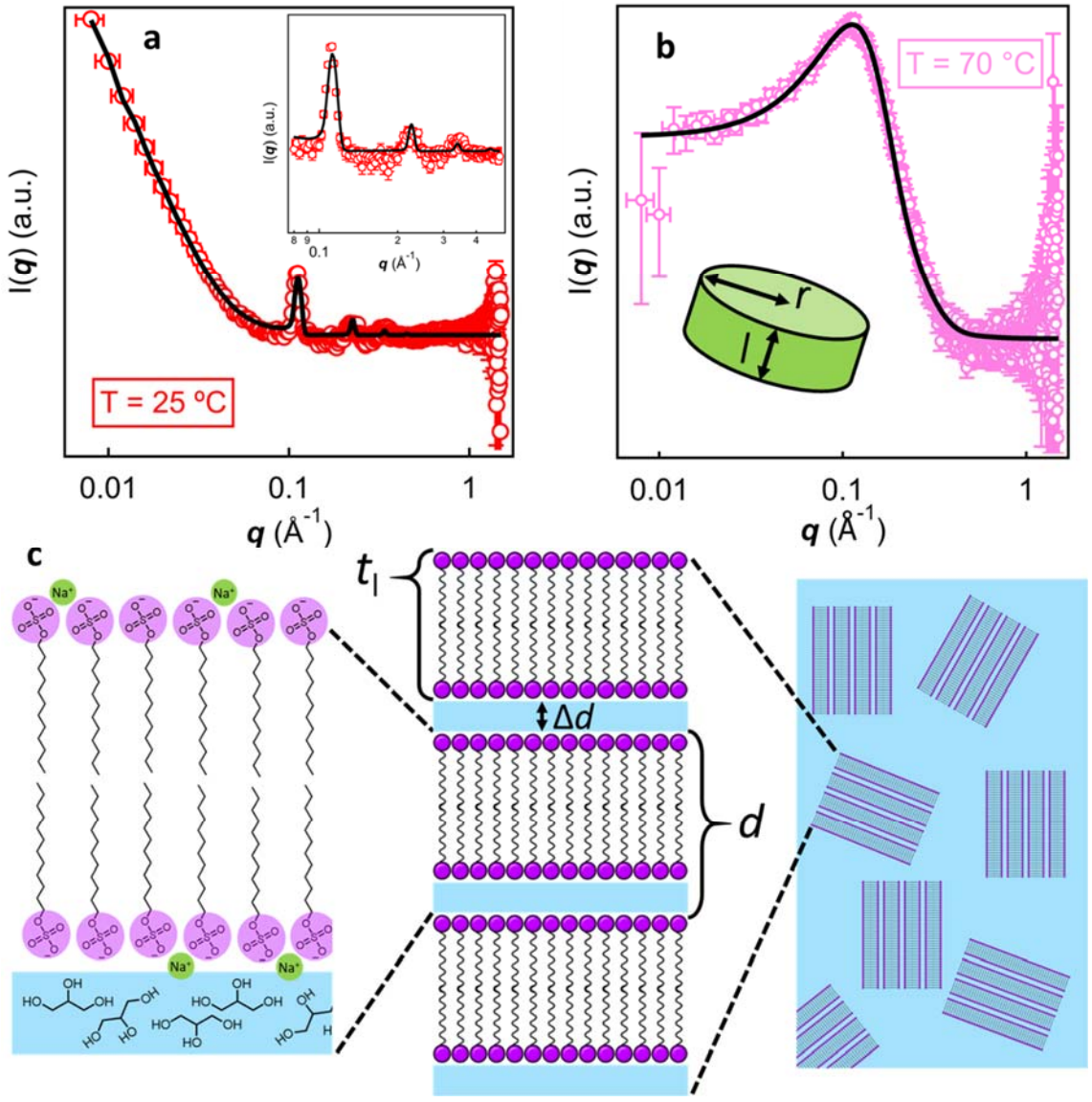

Figure 11 (**a**) Fitted SANS data for 4.4 wt% (~14.7 CMC) *h*-SDS in *d*-glycerol at 25 °C (raw data, red circles; fit, black line) with an enlarged view of the lamellar peaks shown in the inset. (**b**) Fitted SANS data for 4.4 wt% *h*-SDS in *d*-glycerol at 70 °C (raw data, pink circles; fit, black line), with a cartoon depiction of the cylinder morphology (**inset**). (**c**) Schematic representation of the paracrystalline lamellar model used to fit the data at 25 °C.

For the higher temperature data, different micellar aggregate models were trialled, of which a cylindrical form factor with the Hayter-MSA structure factor was found to best fit the SANS profile. **Figure 11b** shows an example fit of this model to the 4.4 wt% SDS-in-glycerol at T = 70 °C (above the CGT ~ 45 °C) with the fitting parameters summarised in **Table 4**. The model describes the globular aggregates as cylindrical in nature, where the interactions between them can be considered as a Coulombic interparticle pair potential[92, 93].

Table 3 Table summarising the fitting parameters for the paracrystalline lamellar stack model used to simulate the data for 4.4 wt% (~14. 7 CMC) *h*-SDS in *d*-glycerol at 25 °C (cf. **Figure 11a**): SDS bilayer thickness t_L, number of layers in the stack n_{Layers}, *d*-spacing, polydispersity of the *d*-spacing σ_d, scattering length density of SDS ρ_{SDS}, scattering length density of glycerol ρ_{Gly}, polydispersity of the SDS bilayer thickness σ_t, and chi squared value χ^2.

Parameter	Lamellar Stack Paracrystal Model
t_L (Å)	48.1
n_{Layers}	21.0
d-Spacing (Å)	55.6
σ_d (Å)	0.01
ρ_{SDS} (10^{-6} Å^{-2})	0.395
ρ_{Gly} (10^{-6} Å^{-2})	7.20
σ_t	0
χ^2	2.62

Table 4 Table summarising the fit parameters for the cylindrical F(***q***) with Hayter-MSA S(***q***) used to simulate the data for 4.4 wt% (~14. 7 CMC) *h*-SDS in *d*-glycerol at 70 °C (cf. **Figure 11b**): scattering length density of SDS ρ_{SDS}, scattering length density of glycerol ρ_{Gly}, cylinder radius *r*, cylinder length *l*, volume fraction φ, charge, temperature *T*, salt concentration c_{salt}, dielectric constant ε, polydispersity of the radius σ_r, polydispersity of the length σ_l, and chi squared value χ^2.

Parameter	Cylindrical F(*q*) with Hayter-MSA S(*q*)
ρ_{SDS} (10^{-6} Å^{-2})	0.395

ρ_{Gly} (10^{-6} Å^{-2})	7.20
r (Å)	17.0
l (Å)	12.0
φ	0.122
Charge (e)	4.94
T (°C)	70 (343 K)
c_{salt} (M)	0
ε	42.5
σ_r	0.229
σ_l	0.234
χ^2	1.39

4. Further discussions and concluding remarks

We have observed the formation of a lamellar, low molecular-weight gel (LMWG) in glycerol, an H-bonding rich nonaqueous polar solvent – at an SDS concentration as low as c_{SDS} ~ 2 wt% (~6.7 CMC), which we have termed the *critical gelation concentration* (*CGC*), below a critical gelation temperature CGT ~ 40-45 °C. This has not been previously reported: it is well established that SDS has a packing parameter of ~ 0.25[94, 95], forming approximately spherical micelles in water at a comparable CMC of c_{SDS} = 2.3-4.4 wt% and 25 °C, whilst an aqueous SDS lamellar phase would form at a much higher c_{SDS} ~ 80 wt% at 60 °C[8, 9].

Our microscopy results showed the presence of anisotropic fibrillar aggregates in gel-like phases, similar in appearance to – but much thicker than – elongated wormlike aggregates with an average diameter, D_a = 0.494 μm, some two orders of magnitude higher compared to ~ 5 nm reported for the wormlike micelle diameter in water. Rheology measurements further indicated the presence of fibrillar aggregates, with shear alignment of the aggregates observed in the σ - $\dot{\gamma}$ plot. The first normal stress difference (N_1) was positive and its magnitude increased with $\dot{\gamma}$, indicating aggregate elongation in the direction of the applied shear, again consistent with the presence of fibrillar aggregates.

SANS measurements showed isotropic scattering at c_{SDS} below ~1 wt%, then above ~2 wt% the scattering profile was well described by a paracrystalline lamellar stack model. Between c_{SDS} ~ 1 – 2 wt% (~ 3.7 – 7.5 CMC) the scattering profile did not show the presence of Bragg peaks or any low-q turnover; hence, the critical gelation concentration is determined to be CGC ~ 1.1 wt% (4.1 CMC). The fitted lamellar thickness, d ~ 55.6 Å, indicated a glycerol layer of Δd ~ 8 Å intercalating with the SDS bilayers (thickness t_L ~ 48.1 Å). This contrasts with SDS in aqueous systems (Figure S8), which typically forms globular micelles at comparable SDS concentrations.

Taken together, nanoscopic structural characterisation from SANS indicates that anisotropically oriented domains of lamellar stacks were the building units in the gel-like phase, which could possibly bundle into fibrillar aggregates observed microscopically. Another possible structure would be a multi-lamellar cylinder, which has been observed in self-assembled structures[96-102], and is analogous to multi-lamellar vesicles observed in aqueous lipid systems. However, the well-defined lamellar spacing means that as the SDS molecular packing (and in turn the elastic property) would have to change in each layer to facilitate a consistent d-spacing, which is an unlikely scenario. To summarise, the link between these lamellar domains and the microfibrillar aggregates remains unclear, and further experiments are required to unravel the structure, *e.g.* using neutron diffraction.

The most striking feature of our observation is the contrast between the self-assembled structures in glycerol and water. To account for the formation of lamellar aggregates using a packing parameter argument, it would be expected that either the tail volume would be much bigger, or the tail length/headgroup area would be much smaller in glycerol. Our surface tensiometry results show a slightly larger (but similar) headgroup area compared to the value in water (46.0 Å^2 *vs* 43.5 Å^2 for glycerol *vs* water), implying a slightly smaller packing parameter which would favour aggregates with a higher curvature. This contrasts with our experimental observation of the lamellar aggregates. Given that the hydrophobic effect (and thus the interfacial tension between the polar solvent and the surfactant tail) is considered the driving force for self-assembly in water, we consider the properties related to the molecular cohesion in glycerol. Such properties, for example, the surface tension (γ) or Hildebrand solubility parameter (δ_h), can be related to the H-bonding in the system, described by either the H-bond capacity (n_{HB}, *i.e.* H-bonding per molecule) or, by considering the molecular volume, the H-bond density (ρ_{HB}) (Table 6).

The material properties of the solvents, such as the boiling point (T_b) and viscosity (η) are higher for glycerol than for water, following the trend in the H-bonding capacity n_{HB}. The viscosity of glycerol is three orders of magnitude higher than that of water (908 cP *vs* 0.89 cP), suggesting that n_{HB} and the molecular architecture contribute to the viscosity. However, **Table 6** shows that the cohesion-dependent parameters track the H-bond density ρ_{HB}, indicating the importance of molecular volume in the H-bond description for self-assembly. This could have implications on fundamental self-assembly concepts, such as the packing parameter, which may need to consider the H-bonding, or intermolecular interactions, to be applied to nonaqueous H-bonding rich solvents.

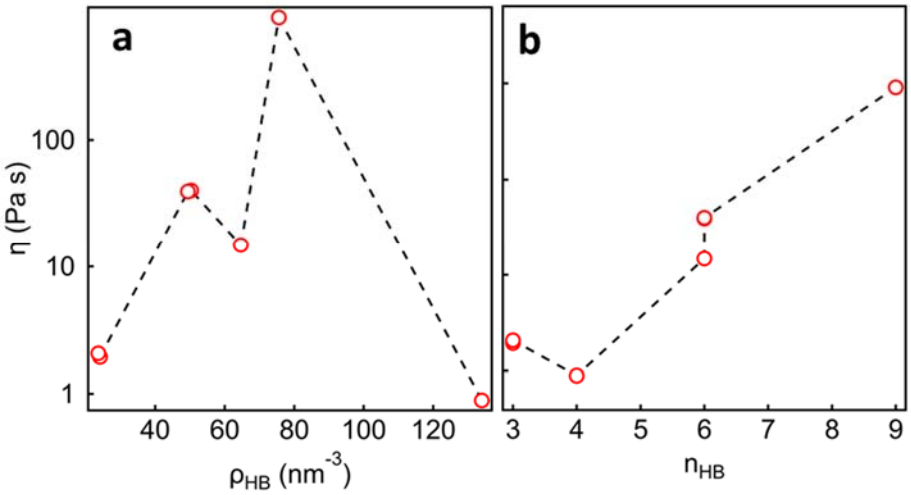

Figure 12 The viscosity, η, of simple alcohols (water, 1-propanol, 2-propanol, 1,2-ethanediol, 1,2-propanediol, 1,3-propanediol, and glycerol) as a function of H-bond density (**a**) and number of H-bonds (**b**).

Table 5 The number of H-bonds, n_{HB}, the H-bond density, ρ_{HB}, and viscosity, η, values for a selection of simple alcohols, plotted graphically in **Figure 13**.

Solvent	n_{HB}	ρ_{HB} (nm^{-3})	η (Pa s)
Water	4	134	0.89[103, 104]
1-Propanol	3	24.1	1.94[105]
2-Propanol	3	23.6	2.07[105]
1,2-Ethanediol	6	64.6	17.0[106]
1,2-Propanediol	6	49.4	44.1[107, 108]
1,3-Propanediol	6	50.3	42.0[107]
Glycerol	9	75.6	908.0[a]

Table 6 A summary of key relevant physical parameters for water and glycerol showing the importance of H-bonding on the system properties: molecular weight (M_w), number of H-bonds (n_{HB}), molecular volume ($V_{molecular}$), H-bond density (ρ_{HB}), density (ρ), boiling point (T_b), viscosity (η), surface tension (γ), Gordon parameter, Hildebrand solubility parameter (δ_H), and dielectric constant (ε). [a] denotes the value has been measured experimentally in this study.

Parameter	Water	Glycerol
M_w (g mol^{-1})	18.0	92.1
N_{HB}	4	9
$V_{molecular}$ (Å^3)	30	120
P_{HB} (nm^{-3})	134	76
P (25 °C, g cm^{-3})	1.00[103]	1.26[103]
T_b (K)	373[109]	563[109]
H (25 °C, cP)	0.89[103, 104]	908[a]
Γ (25 °C, mN m^{-1})	72.8[110]	64.0[a]
Gordon parameter (J m^{-3})	2.74-2.8[104, 111, 112]	1.51[111, 112]
Δ_h (J m^{-3})	16.7[109, 113]	14.3[109, 113]
E (25 °C, F m^{-1})	78.5[109, 110]	42.5[109]

Further experimental work, such as neutron diffraction and rheo-SANS, would be required to fully resolve the molecular packing in the aggregate structure. Our results have demonstrated that the established concepts in molecular self-assembly for aqueous systems cannot be applied fully to this curious case of SDS self-assembly in glycerol. Understanding the mechanism behind such self-assembled structures will be important to many applications from personal care products and drug delivery methods using glycerol, to the fundamental role of glycerol in biological processes (e.g. the heightened level of glycerol in the blood of *hyalophoria cecropia* pupae during diapause).

Acknowledgements

We acknowledge the ISIS Muon and Neutron Source for the awarded beamtime under experiment numbers: RB 1810629 and RB 1910080; data available under

10.5286/ISIS.E.RB1810629 and 10.5286/ISIS.E.RB1910080 respectively. We thank S. Michel, S. Ruscigno, and B. Bharatiya for their help with the SANS experiments. We also acknowledge the MRC in addition to the Wolfson Foundation for establishing the Wolfson Bioimaging Facility, University of Bristol, for use of their confocal and scanning electron microscopes. We would like to acknowledge Dr Alan Leard and Dr Judith Mantell for their support with use of the microscopes in the Wolfson Bioimaging Facility. Lastly, we would like to acknowledge the Engineering and Physical Science Research Council (EPSRC) and GlaxoSmithKline for providing the funding for L. Matthews, through the Bristol Centre for Functional Nanomaterials (EPSRC, EP/L016648/1). SasView, originally developed under NSF award DMR-0520547, contains code developed with funding from the European Union's Horizon 2020 research and innovation programme under the SINE2020 project, grant agreement No 654000.

References

1. H. Chino, *Nature*, 1957, **180**, 606-607.
2. H. Chino, *J Insect Physiol*, 1958, **2**, 1-12.
3. P. Dubach, D. Pratt, F. Smith and C. M. Stewart, *Nature*, 1959, **184**, 288-289.
4. R. W. Salt, *Nature*, 1958, **181**, 1281-1281.
5. G. R. Wyatt and W. L. Meyer, *J Gen Physiol*, 1959, **42**, 1005-1011.
6. C. von Ferber and H. Lowen, *Faraday Discuss*, 2005, **128**, 389-405.
7. B. Cabane, R. Duplessix and T. Zemb, *J Phys-Paris*, 1985, **46**, 2161-2178.
8. P. Kekicheff, *Journal of colloid and interface science*, 1989, **131**, 133-152.
9. P. Kekicheff, C. Grabiellemadelmont and M. Ollivon, *Journal of colloid and interface science*, 1989, **131**, 112-132.
10. G. Montalvo, M. Valiente and E. Rodenas, *Journal of colloid and interface science*, 1995, **172**, 494-501.
11. N. J. Chang and E. W. Kaler, *J Phys Chem-Us*, 1985, **89**, 2996-3000.
12. N. A. Mazer, G. B. Benedek and M. C. Carey, *J Phys Chem-Us*, 1976, **80**, 1075-1085.
13. K. J. Mysels and L. H. Princen, *J Phys Chem-Us*, 1959, **63**, 1696-1700.
14. M. A. Hillmyer, F. S. Bates, K. Almdal, K. Mortensen, A. J. Ryan and J. P. A. Fairclough, *Science*, 1996, **271**, 976-978.
15. A. S. Poulos, C. S. Jones and J. T. Cabral, *Soft Matter*, 2017, **13**, 5332-5340.
16. C. Tanford, *The hydrophobic effect: Formation of micelles and biological membranes*, Wiley & Sons, New York, US, Second edn., 1976.
17. C. Tanford, *Science*, 1978, **200**, 1012-1018.
18. J. Israelachvili, *Colloids and Surfaces a-Physicochemical and Engineering Aspects*, 1994, **91**, 1-8.
19. J. Israelachvili and R. Pashley, *Nature*, 1982, **300**, 341-342.
20. J. N. Israelachvili, D. J. Mitchell and B. W. Ninham, *J Chem Soc Farad T 2*, 1976, **72**, 1525-1568.
21. J. N. Israelachvili and R. M. Pashley, *Nature*, 1983, **306**, 249-250.

22. H. Khan, J. M. Seddon, R. V. Law, N. J. Brooks, E. Robles, J. T. Cabral and O. Ces, *Journal of colloid and interface science*, 2019, **538**, 75-82.
23. R. A. Abdel-Rahem, *J. Dispersion Sci. Technol.*, 2013, **34**, 932-940.
24. X. Auvray, T. Perche, R. Anthore, C. Petipas, I. Rico and A. Lattes, *Langmuir*, 1991, **7**, 2385-2393.
25. C. Seguin, J. Eastoe, R. K. Heenan and I. Grillo, *Langmuir*, 2007, **23**, 4199-4202.
26. C. Seguin, J. Eastoe, R. K. Heenan and I. Grillo, *Journal of colloid and interface science*, 2007, **315**, 714-720.
27. C. Seguin, J. Eastoe, S. Rogers, M. Hollamby and R. M. Dalgliesh, *Langmuir*, 2006, **22**, 11187-11192.
28. C. Seguin, J. Eastoe, R. Clapperton, R. K. Heenan and I. Grillo, *Colloids and Surfaces a-Physicochemical and Engineering Aspects*, 2006, **282**, 134-142.
29. C. C. Ruiz, L. Diaz-Lopez and J. Aguiar, *J. Dispersion Sci. Technol.*, 2008, **29**, 266-273.
30. H. A. Barnes, *A Handbook of Elementary Rheology*, The University of Wales Institute of Non-Newtonian Fluid Mechanics, Aberystwyth, UK, First edn., 2000.
31. P. B. Heenan, *New Zeal J Bot*, 1997, **35**, 395-415.
32. T. Heenan, *Overland*, 1997, **146**, 5-12.
33. C. C. Ruiz, *Colloid Polym Sci*, 1999, **277**, 701-707.
34. R. K. Heenan, S. E. Rogers, D. Turner, A. E. Terry, J. Treadgold and S. M. King, *Neutron News*, 2011, **22**, 19-21.
35. R. K. Heenan, S. M. King, R. Osborn and H. B. Stanley, *COLETTE Users Guide*, Rutherford Appleton Laboratory Report, 1989.
36. S. M. King and R. K. Heenan, *Using COLETTE*, Rutherford Appleton Laboratory Report, 1995.
37. G. D. Wignall and F. S. Bates, *J Appl Crystallogr*, 1987, **20**, 28-40.
38. J. Berghausen, J. Zipfel, P. Lindner and W. Richtering, *J. Phys. Chem. B*, 2001, **105**, 11081-11088.
39. F. Nallet, R. Laversanne and D. Roux, *J Phys Ii*, 1993, **3**, 487-502.
40. M. Bergstrom, J. S. Pedersen, P. Schurtenberger and S. U. Egelhaaf, *J. Phys. Chem. B*, 1999, **103**, 9888-9897.
41. A. Caille, *Cr Acad Sci B Phys*, 1972, **274**, 891-893.
42. A. Guinier and G. Fournet, *Small-Angle Scattering of X-Rays*, John Wiley & Sons, Inc., New York, US, 1955.
43. J. S. Pedersen, *Adv Colloid Interfac*, 1997, **70**, 171-210.
44. A. Slastanova, R. A. Campbell, T. Snow, E. Mould, P. Li, R. J. L. Welbourn, M. Chen, E. Robles and W. H. Briscoe, *J Colloid Interface Sci*, 2020, **561**, 181-194.
45. A. Z. Cardoso, L. L. E. Mears, B. N. Cattoz, P. C. Griffiths, R. Schweins and D. J. Adams, *Soft Matter*, 2016, **12**, 3612-3621.
46. L. Chen, G. Pont, K. Morris, G. Lotze, A. Squires, L. C. Serpell and D. J. Adams, *Chemical Communications*, 2011, **47**, 12071-12073.
47. E. R. Draper and D. J. Adams, *Chem-Us*, 2017, **3**, 390-410.
48. S. R. Raghavan and J. F. Douglas, *Soft Matter*, 2012, **8**, 8539-8546.
49. K. Trickett and J. Eastoe, *Adv Colloid Interfac*, 2008, **144**, 66-74.
50. J. Yang, *Curr Opin Colloid In*, 2002, **7**, 276-281.
51. D. P. Acharya and H. Kunieda, *Adv Colloid Interfac*, 2006, **123**, 401-413.
52. X. M. Pei, J. X. Zhao and X. L. Wei, *Journal of colloid and interface science*, 2011, **356**, 176-181.

53. X. M. Pei, J. X. Zhao, Y. Z. Ye, Y. You and X. L. Wei, *Soft Matter*, 2011, **7**, 2953-2960.
54. R. G. Shrestha, L. K. Shrestha and K. Aramaki, *Journal of colloid and interface science*, 2008, **322**, 596-604.
55. T. M. Clausen, P. K. Vinson, J. R. Minter, H. T. Davis, Y. Talmon and W. G. Miller, *J Phys Chem-Us*, 1992, **96**, 474-484.
56. A. Khatory, F. Lequeux, F. Kern and S. J. Candau, *Langmuir*, 1993, **9**, 1456-1464.
57. A. L. Kwiatkowski, V. S. Molchanov, A. S. Orekhov, A. L. Vasiliev and O. E. Philippova, *J. Phys. Chem. B*, 2016, **120**, 12547-12556.
58. Z. Lin, J. J. Cai, L. E. Scriven and H. T. Davis, *J Phys Chem-Us*, 1994, **98**, 5984-5993.
59. J. F. Berret, *Langmuir*, 1997, **13**, 2227-2234.
60. J. F. Berret, J. Appell and G. Porte, *Langmuir*, 1993, **9**, 2851-2854.
61. H. Mohammadigoushki and S. J. Muller, *Soft Matter*, 2016, **12**, 1051-1061.
62. A. V. Shibaev, V. S. Molchanov and O. E. Philippova, *J. Phys. Chem. B*, 2015, **119**, 15938-15946.
63. N. A. Spenley, M. E. Cates and T. C. B. Mcleish, *Physical review letters*, 1993, **71**, 939-942.
64. R. Miki, C. Takei, Y. Ohtani, K. Kawashima, A. Yoshida, Y. Kojima, Y. Egawa, T. Seki, D. Iohara, M. Anraku, F. Hirayama and K. Uekama, *Molecular Pharmaceutics*, 2018, **15**, 1097-1104.
65. N. Zoratto, I. Grillo, P. Matricardi and C. A. Dreiss, *Journal of colloid and interface science*, 2019, **556**, 301-312.
66. J. R. Chen, N. E. Clay, N. H. Park and H. Kong, *Chem Eng Sci*, 2015, **125**, 20-24.
67. C. A. Dreiss, *Soft Matter*, 2007, **3**, 956-970.
68. S. Hayashi and S. Ikeda, *J Phys Chem-Us*, 1980, **84**, 744-751.
69. G. Garg, P. A. Hassan, V. K. Aswal and S. K. Kulshreshtha, *J. Phys. Chem. B*, 2005, **109**, 1340-1346.
70. T. Goel, M. K. Umbhakar, T. Mukherjee and H. Pal, *J Photoch Photobio A*, 2010, **209**, 41-48.
71. P. A. Hassan, G. Fritz and E. W. Kaler, *Journal of colloid and interface science*, 2003, **257**, 154-162.
72. M. R. Rojas, A. J. Muller and A. E. Saez, *Journal of colloid and interface science*, 2010, **342**, 103-109.
73. R. H. Colby, D. C. Boris, W. E. Krause and S. Dou, *Rheol Acta*, 2007, **46**, 569-575.
74. R. G. Larson, *Rheol Acta*, 1992, **31**, 213-263.
75. R. G. Larson and P. S. Desai, *Annu Rev Fluid Mech*, 2015, **47**, 47-65.
76. T. C. O'Connor, N. J. Alvarez and M. O. Robbins, *Physical review letters*, 2018, **121**, 1-6.
77. R. I. Tanner, *Engineering Rheology*, Oxford University Press, Oxford, UK, 1985.
78. S. Khandavalli, J. Hendricks, C. Clasen and J. P. Rothstein, *J Rheol*, 2016, **60**, 1331-1346.
79. A. Tavera-Vazquez, B. Arenas-Gomez, C. Garza, Y. Liu and R. Castillo, *Soft Matter*, 2018, **14**, 7264-7276.
80. M. W. Liberatore, F. Nettesheim, P. A. Vasquez, M. E. Helgeson, N. J. Wagner, E. W. Kaler, L. P. Cook, L. Porcar and Y. T. Hu, *J Rheol*, 2009, **53**, 441-458.
81. F. C. Mackintosh, J. Kas and P. A. Janmey, *Physical review letters*, 1995, **75**, 4425-4428.
82. F. Gittes, B. Mickey, J. Nettleton and J. Howard, *J Cell Biol*, 1993, **120**, 923-934.
83. M. Czerner, L. S. Fellay, M. P. Suarez, P. M. Frontini and L. A. Fasce, *Proc Mat Sci*, 2015, **8**, 287-296.
84. B. A. Schubert, E. W. Kaler and N. J. Wagner, *Langmuir*, 2003, **19**, 4079-4089.

85. D. P. Acharya, D. Varade and K. Aramaki, *Journal of colloid and interface science*, 2007, **315**, 330-336.
86. P. A. Hassan, S. J. Candau, F. Kern and C. Manohar, *Langmuir*, 1998, **14**, 6025-6029.
87. R. Kumar, G. C. Kalur, L. Ziserman, D. Danino and S. R. Raghavan, *Langmuir*, 2007, **23**, 12849-12856.
88. H. Rehage and H. Hoffmann, *Molecular Physics*, 1991, **74**, 933-973.
89. R. G. Shrestha, K. Nomura, M. Yamamoto, Y. Yamawaki, Y. Tamura, K. Sakai, K. Sakamoto, H. Sakai and M. Abe, *Langmuir*, 2012, **28**, 15472-15481.
90. F. E. Antunes, L. Gentile, C. O. Rossi, L. Tavano and G. A. Ranieri, *Colloids and Surfaces B-Biointerfaces*, 2011, **87**, 42-48.
91. S. S. Berr and R. R. M. Jones, *Langmuir*, 1988, **4**, 1247-1251.
92. J. P. Hansen and J. B. Hayter, *Molecular Physics*, 1982, **46**, 651-656.
93. J. B. Hayter and J. Penfold, *Molecular Physics*, 1981, **42**, 109-118.
94. G. B. Ray, I. Chakraborty, S. Ghosh and S. P. Moulik, *Colloid Polym Sci*, 2007, **285**, 457-469.
95. C. Tanford, *J Phys Chem-Us*, 1972, **76**, 3020-3024.
96. S. Fujii and Y. Yamamoto, *Soft Matter*, 2015, **11**, 9330-9341.
97. J. Landman, S. Ouhajji, S. Prevost, T. Narayanan, J. Groenewold, A. P. Philipse, W. K. Kegel and A. V. Petukhov, *Sci Adv*, 2018, **4**.
98. Z. W. Yuan, Z. L. Yin, S. X. Sun and J. C. Hao, *J. Phys. Chem. B*, 2008, **112**, 1414-1419.
99. L. Gentile, M. A. Behrens, L. Porcar, P. Butler, N. J. Wagner and U. Olsson, *Langmuir*, 2014, **30**, 8316-8325.
100. F. Nettesheim, J. Zipfel, U. Olsson, F. Renth, P. Lindner and W. Richtering, *Langmuir*, 2003, **19**, 3603-3618.
101. C. D. Santangelo and P. Pincus, *Physical Review E*, 2002, **66**, 1-7.
102. T. Shimizu, M. Masuda and H. Minamikawa, *Chem Rev*, 2005, **105**, 1401-1443.
103. I. I. Adamenko, L. A. Bulavin, V. Ilyin, S. A. Zelinsky and K. O. Moroz, *J Mol Liq*, 2006, **127**, 90-92.
104. J. Kestin, M. Sokolov and W. A. Wakeham, *J Phys Chem Ref Data*, 1978, **7**, 941-948.
105. F. M. Pang, C. E. Seng, T. T. Teng and M. H. Ibrahim, *J Mol Liq*, 2007, **136**, 71-78.
106. W. Hayduk and V. K. Malik, *J Chem Eng Data*, 1971, **16**, 143-146.
107. D. M. Bajic, G. R. Ivanis, Z. P. Visak, E. M. Zivkovic, S. P. Serbanovic and M. L. Kijevcanin, *J Chem Thermodyn*, 2013, **57**, 510-529.
108. T. F. Sun and A. S. Teja, *J Chem Eng Data*, 2004, **49**, 1311-1317.
109. A. Wolfson, C. Dlugy and Y. Shotland, *Environ Chem Lett*, 2007, **5**, 67-71.
110. N. B. Vargaftik, B. N. Volkov and L. D. Voljak, *J Phys Chem Ref Data*, 1983, **12**, 817-820.
111. A. H. Beesley, D. F. Evans and R. G. Laughlin, *J Phys Chem-Us*, 1988, **92**, 791-793.
112. T. L. Greaves and C. J. Drummond, *Chemical Society Reviews*, 2008, **37**, 1709-1726.
113. C. M. Hansen, *Ind Eng Chem Prod Rd*, 1969, **8**, 2-&.

Supporting Materials (SM)

The curious case of SDS self-assembly in glycerol: *Formation of a lamellar gel*

Lauren Matthews[1,2], Zaneta Przybyowicz[1], Sarah E. Rogers[3], Paul Bartlett[1], Andrew J. Johnson[4], Robert Sochon[4], and Wuge H. Briscoe[1]*

[1] School of Chemistry, University of Bristol, Cantock's Close, Bristol BS8 1TS, UK

[2] Bristol Centre for Functional Nanomaterials, HH Wills Physics Laboratory, University of Bristol, Tyndall Avenue, Bristol BS8 1TL, UK

[3] ISIS Neutron and Muon Source, Rutherford Appleton Laboratory, Harwell Oxford, Didcot, OX11 0QX, UK

[3] GlaxoSmithKline, St George's Avenue, Weybridge, KT13 0DE, UK

*Corresponding author; email: wuge.briscoe@bristol.ac.uk; Tel: +44 (0)117 3318256

S1. General observations of gelation

The effect of concentration was investigated by preparing a series of SDS and glycerol mixtures at various SDS concentrations. Each of the samples was similarly prepared, where the mixture was agitated at 550 RPM at 60 ^{o}C. **Table S1** summarises the results from vial inversion tests: if the sample held its weight upon inversion, it was deemed a positive result. **Table S1** shows that the gel only started to form at ~ 1.1 wt % SDS, with full gelation occurring at ~2.3 wt % SDS.

Table S1 Physical observations from the vial inversion tests at different SDS concentrations. **N** denotes a transparent phase that flowed upon inversion formed. **Y** denotes an opaque phase that held its weight upon inversion. **N[a]** denotes that the sample started to thicken, but the phase still flowed upon vial inversion.

SDS wt %	0.0	0.2	0.6	1.1	2.3	2.7	3.1	3.5	4.0	4.4	4.8
Vial Inversion Result	N	N	N	N[a]	Y	Y	Y	Y	Y	Y	Y

Heating and agitation of SDS and glycerol mixtures was an important step in producing the gel mesophase, and thus, the effect of these variables was probed. The mixtures were tested as above with a series of vial inversion tests, at different concentrations and using different preparation methods, and the results are summarised in **Table S2**. It can be seen that the sample preparation method is important to whether the gel is produced, likely due to the system needing to overcome a kinetic energy barrier.

Table S2 Further physical observations from varying sample preparation of SDS in glycerol. **N** is neither heated nor agitated, **H** is heated only, **S** is agitated only, **H/S** is both heated and agitated. **N** denotes a transparent phase that flowed upon inversion. **Y** denotes an opaque phase that held its weight upon inversion. **N[a]** denotes that the sample started to thicken, but still flowed upon vial inversion. **N[b]** denotes that the sample contained solvated crystals.

SDS wt %	Glycerol			
	N	H	S	H/S
0.2	N	--	--	N
0.6	N	--	--	N
1.1	N	--	--	N[a]
2.3	N[b]	N	N	Y
4.4	N[b]	N[a]	N[a]	Y

The effect of temperature was also investigated, using small-angle neutron scattering (SANS), where SDS and glycerol mixtures were measured at different concentrations and temperatures. The positive result for a gel phase was the distinctive scattering pattern containing the three lamellar Bragg peaks shown in **Figure 7a** (red curve, main text), and the results from these checks are shown in **Table S3**. The effect of temperature can be seen clearly here, as with increasing temperature to ~ 45-50 ^{o}C, the phase underwent a transition to a micellar phase (**Figure 8**, main text), reminiscent of that observed in aqueous media.

Table S3 Summary of the effect of temperature on the SDS and glycerol mixtures from SANS measurements. **N** denotes the scattering data consisting of a micellar pattern. **Y** denotes the scattering data consisting of a lamellar pattern. **25[a]** denotes that the sample had been cooled to 25 ^{o}C and measured after two hours. **25[b]** denotes that the sample had been cooled to 25 ^{o}C and measured after four hours. **25[c]** denotes that the sample had been cooled to 25 ^{o}C and measured after being left overnight. **N[d]** denotes that scattering pattern was closer to an isotropic pattern (flat scattering) as opposed to a micellar pattern. **N[e]** denotes that the pattern had no turnover at low *q*, but also did not contain the Bragg peaks.

SDS wt %	Temperature (°C)											
	25	35	40	45	50	55	60	65	70	25[a]	25[b]	25[c]
0.2	N[d]	--	N[d]	--	--	--	--	--	N[d]	--	--	--
0.6	N[d]	--	N[d]	--	--	--	--	--	N[d]	--	--	--
1.1	Y	--	Y	N	N	--	--	--	N	N	Y	--
2.3	Y	Y	Y	--	N	N	N	N	N	N	Y	Y
4.4	Y	Y	Y	--	N	N	N	N	N	N[e]	Y	Y

S2. Further rheology characterisation for the SDS-in-glycerol gel

The first normal stress difference (N_1) as a function of the shear rate is shown in the main text as the **inset** of **Figure 6**, and here plotted on a log-log scale with a slope ~ 3.8.

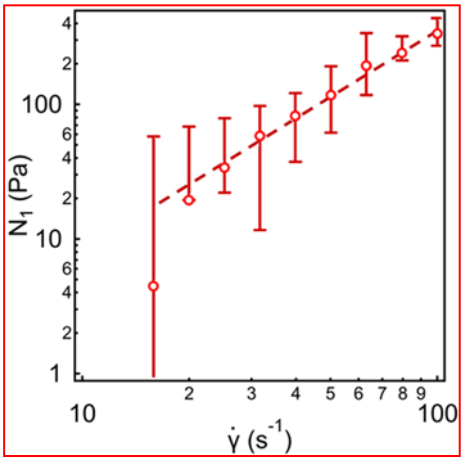

Figure S1 First normal stress difference, N_1, *vs* shear rate, $\dot{\gamma}$, for the SDS-in-glycerol gel (4.4 wt%; ~14.7 CMC) plotted on a log-log scale. The negative values in **Figure 6** have been removed for this plot. A linear dependence is observed with a slope ~ 3.8.

S3. Model refinement for SANS data fitting of the SDS-in-glycerol gel at 25 °C

The Bragg peaks of the SDS and glycerol gel indicated the formation of a lamellar phase, taken from the relative ***q*** positions (**Table S4**). The physical parameters of this lamellar phase were probed using a model analysis; a selection of lamellar models in the SasView application were tested to provide the most appropriate model for the system. The models were initially fitted primitively with the idealised parameters and then the best candidates were chosen for further refinement.

Table S4 Bragg peak positions for the SDS-in-glycerol gel at the two highest surfactant concentrations (4.4 and 2.3 wt%).

Conc (wt%)	Peak	q (Å^{-1})	d-Spacing (Å)
4.4	1	0.11	57.1
	2	0.22	57.1
	3	0.34	55.4
2.3	1	0.11	57.1
	2	0.22	57.1
	3	0.33	57.1

Figure S2 shows the initial primitive fits for the various lamellar models using 4.4 wt% SDS in glycerol as an example system, with tables summarising the fitting parameters for each (**Table S5** - **Table S9**). From the physical appearance of the fits and the values of the statistical 'goodness of fit' parameter, χ^2, the models that fit the SANS profile the best were the lamellar stack model with Caillé S(q) and the lamellar paracrystal stack model. These two models were then further refined to obtain the model best suited for the SANS profile. For clarity, the meaning of the fitting parameters in the different models listed below are as follows:

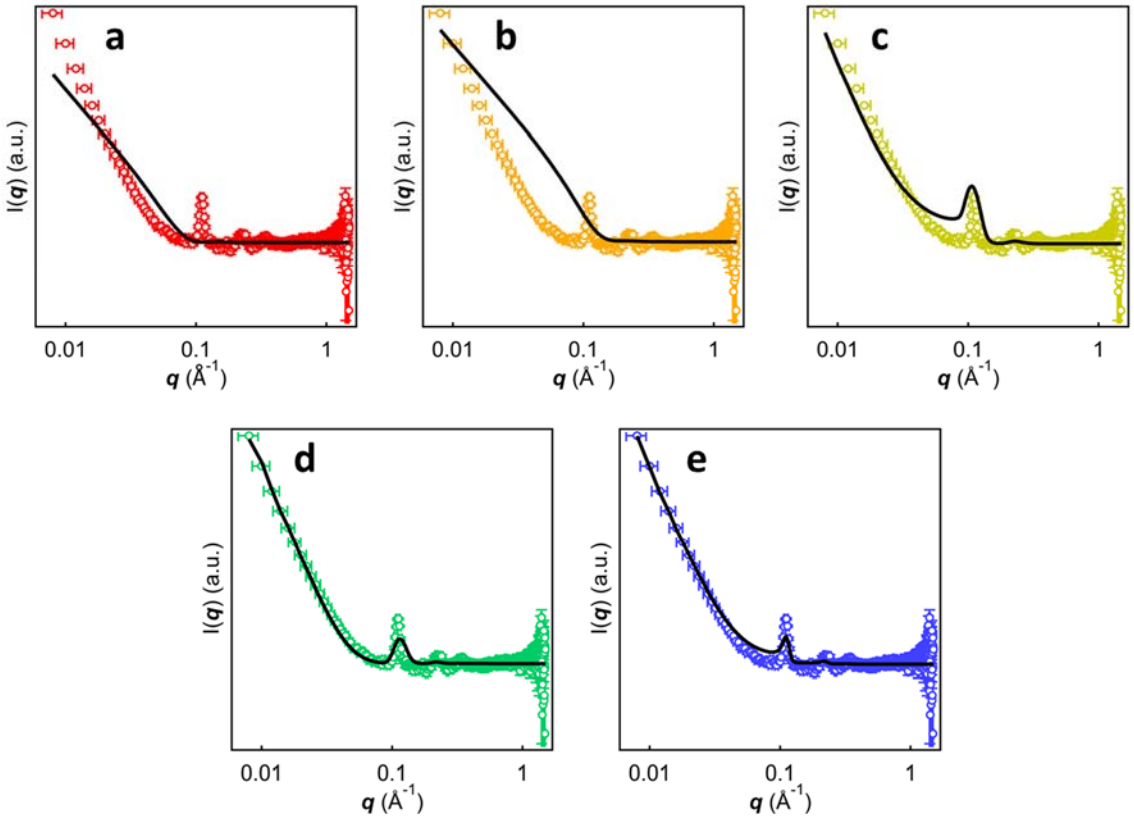

Figure S2 Fitted SANS data for 4.4 wt% SDS in glycerol at 25 °C using: (**a**) a simple lamellar stack model; (**b**) the lamellar stack model with separated headgroup and tail contributions; (**c**) the lamellar stack model with Caillé S(***q***) and separated headgroup and tail contributions; (**d**) the lamellar stack model with Caillé S(***q***); and (**e**) the lamellar paracrystal stack model.

Table S5 A summary of the fitting parameters for 4.4 wt% SDS in glycerol at 25 °C using a simple lamellar stack model: SDS bilayer thickness t_L, scattering length density of SDS ρ_{SDS}, scattering length density of glycerol ρ_{Gly}, polydispersity of the SDS bilayer thickness σ_t, and chi squared value χ^2.

Parameter	Lamellar Stack Model
Scale (10^{-3})	0.987
Background (cm^{-1})	0.121
t_L (Å)	55.6
ρ_{SDS} (10^{-6} Å^{-2})	0.395
ρ_{Gly} (10^{-6} Å^{-2})	7.20
σ_t	0.1
χ^2	98.6

Table S6 A summary of the fitting parameters for 4.4 wt% SDS in glycerol at 25 °C using the lamellar stack model with separated headgroup and tail contributions: SDS headgroup thickness t_{head}, SDS tail thickness t_{tail}, scattering length density of the SDS headgroup ρ_{HG}, scattering length density of the SDS tails ρ_{tail}, scattering length density of glycerol ρ_{Gly}, polydispersity of the SDS headgroup thickness σ_{head}, polydispersity of the SDS tail thickness σ_{tail}, and chi squared value χ^2.

Parameter	Lamellar Stack Model with Separate HG and Tail
Scale (10^{-3})	5.95
Background (cm^{-1})	0.124
t_{head} (Å)	4.00
t_{tail} (Å)	17.0
ρ_{HG} (10^{-6} Å^{-2})	-0.391
ρ_{tail} (10^{-6} Å^{-2})	5.11
ρ_{Gly} (10^{-6} Å^{-2})	7.20
σ_{head}	0.172
σ_{tail}	0.05
χ^2	1570

Table S7 A summary of the fitting parameters for 4.4 wt% SDS in glycerol at 25 °C using the lamellar stack model with Caillé S(q) and separated headgroup and tail contributions: SDS headgroup thickness t_{head}, SDS tail thickness t_{tail}, number of SDS layers n_{layers}, d-Spacing, Caillé parameter, scattering length density of the SDS headgroup ρ_{HG}, scattering length density of the SDS tails ρ_{tail}, scattering length density of glycerol ρ_{Gly}, polydispersity of the SDS headgroup thickness σ_{head}, polydispersity of the SDS tail thickness σ_{tail}, polydispersity of the d-Spacing thickness $\sigma_{d\text{-}Spacing}$, and chi squared value χ^2.

Parameter	Lamellar Stack Model with Caillé S(q) and Separate HG and Tail
Scale (10^{-3})	1.48
Background (cm^{-1})	0.116
t_{head} (Å)	4.00

t_{tail} (Å)	17.0
n_{layers}	30.0
d-Spacing (Å)	55.6
Caillé Param. (Å^{-2})	0.158
ρ_{HG} (10^{-6} Å^{-2})	-0.391
ρ_{tail} (10^{-6} Å^{-2})	5.11
ρ_{Gly} (10^{-6} Å^{-2})	7.20
σ_{head}	0.10
σ_{tail}	0.10
$\sigma_{d\text{-}Spacing}$	0.10
χ^2	71.3

Table S8 A summary of the fitting parameters for 4.4 wt% SDS in glycerol at 25 °C using the lamellar stack model with Caillé S(***q***): SDS bilayer thickness t_L, number of SDS layers n_{layers}, d-Spacing, Caillé parameter, scattering length density of the SDS bilayer ρ_{SDS}, scattering length density of glycerol ρ_{Gly}, polydispersity of the SDS bilayer thickness σ_t, polydispersity of the d-Spacing thickness $\sigma_{d\text{-}Spacing}$, and chi squared value χ^2.

Parameter	Lamellar Stack Model with Caillé S(q)
Scale (10^{-3})	6.71
Background (cm^{-1})	0.123
t_L (Å)	69.4
n_{layers}	20.0
d-Spacing (Å)	55.6
ρ_{SDS} (10^{-6} Å^{-2})	0.395
ρ_{Gly} (10^{-6} Å^{-2})	7.20
σ_t	0.10
$\sigma_{d\text{-}Spacing}$	0.10
χ^2	5.82

Table S9 A summary of the fitting parameters for 4.4 wt% SDS in glycerol at 25 °C using the lamellar paracrystal stack model: SDS bilayer thickness t_L, number of layers in the stack n_{Layers}, *d*-spacing, polydispersity of the *d*-spacing σ_d, scattering length density of SDS ρ_{SDS}, scattering length density of glycerol ρ_{Gly}, polydispersity of the SDS bilayer thickness σ_t, polydispersity of the d-Spacing thickness $\sigma_{d\text{-}Spacing}$, and chi squared value χ^2.

Parameter	Lamellar Paracrystal Stack Model
Scale	0.610
Background (cm^{-1})	0.120
t_L (Å)	69.4
n_{layers}	22.6
d-Spacing (Å)	55.6
ρ_{SDS} (10^{-6} Å^{-2})	0.395
ρ_{Gly} (10^{-6} Å^{-2})	7.20
σ_t	0.10
$\sigma_{d\text{-}Spacing}$	0.10
χ^2	4.73

Further refinement of the SANS data using the two models showed that the two models fitted well to the raw SANS profile (**Figure S3**). However, the lamellar paracrystal stack did track the SANS profile better, as reflected in both the χ^2 value and the physical appearance. The lamellar paracrystal stack model was thus chosen as the most appropriate model to describe the SANS profile of the gel mesophase.

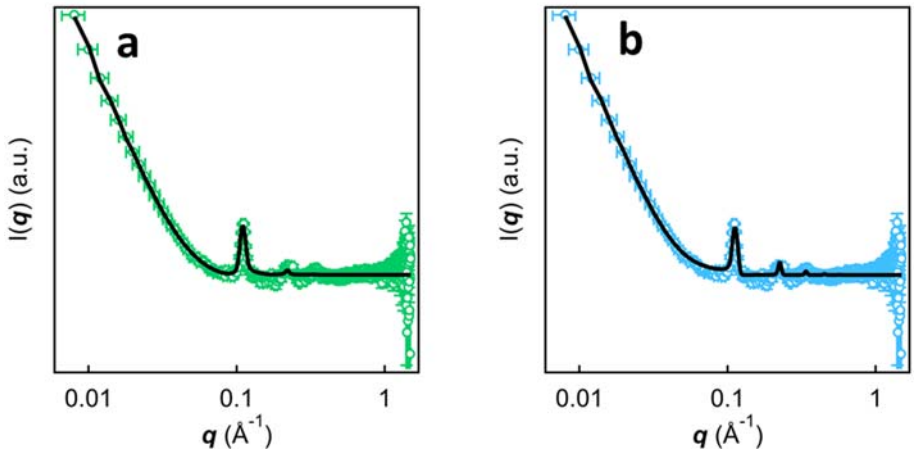

Figure S3 Further refined fitted SANS data for 4.4 wt% SDS in glycerol at 25 °C using: (**a**) the lamellar stack model with Caillé S(***q***); and (**b**) the lamellar paracrystal stack model.

Table S10 A summary of the further refined fitting parameters for 4.4 wt% SDS in glycerol at 25 °C using the lamellar stack model with Caillé S(***q***): SDS bilayer thickness t_L, number of SDS layers n_{layers}, d-Spacing, Caillé parameter, scattering length density of the SDS bilayer ρ_{SDS}, scattering length density of glycerol ρ_{Gly}, polydispersity of the SDS bilayer thickness σ_t, polydispersity of the d-Spacing thickness $\sigma_{d\text{-}Spacing}$, and chi squared value χ^2.

Parameter	Lamellar Stack Model with Caillé S(*q*)
Scale (10^{-3})	6.90
Background (cm^{-1})	0.123
t_L (Å)	69.5
n_{layers}	20.0
d-Spacing (Å)	57.0
ρ_{SDS} (10^{-6} Å^{-2})	0.300
ρ_{Gly} (10^{-6} Å^{-2})	7.30
σ_t	0.10
$\sigma_{d\text{-}Spacing}$	0.00
χ^2	2.77

Table S11 A summary of the further refined fitting parameters for 4.4 wt% SDS in glycerol at 25 °C using the lamellar paracrystal stack model: SDS bilayer thickness t_L, number of layers in the stack n_{Layers}, *d*-spacing, polydispersity of the *d*-spacing σ_d, scattering length density of SDS

ρ_{SDS}, scattering length density of glycerol ρ_{Gly}, polydispersity of the SDS bilayer thickness σ_t, polydispersity of the d-Spacing thickness $\sigma_{d\text{-}Spacing}$, and chi squared value χ^2.

Parameter	Lamellar Paracrystal Stack Model
Scale	0.613
Background (cm^{-1})	0.122
t_L (Å)	48.1
n_{layers}	21.0
d-Spacing (Å)	55.6
ρ_{SDS} (10^{-6} Å^{-2})	0.395
ρ_{Gly} (10^{-6} Å^{-2})	7.20
σ_t	0.01
$\sigma_{d\text{-}Spacing}$	0.00
χ^2	2.61

S3. Fitted SANS data for the SDS-in-glycerol gel at 25 ºC

Figure S4 shows the fitted SANS profiles for the SDS-in-glycerol gel for the different SDS concentrations measured, fitted to the lamellar paracrystal stack model as shown previously. The model is shown to be appropriate for the concentrations measured. The values of the fitted parameters are identical between the two concentrations measured, suggesting that the morphology did not change.

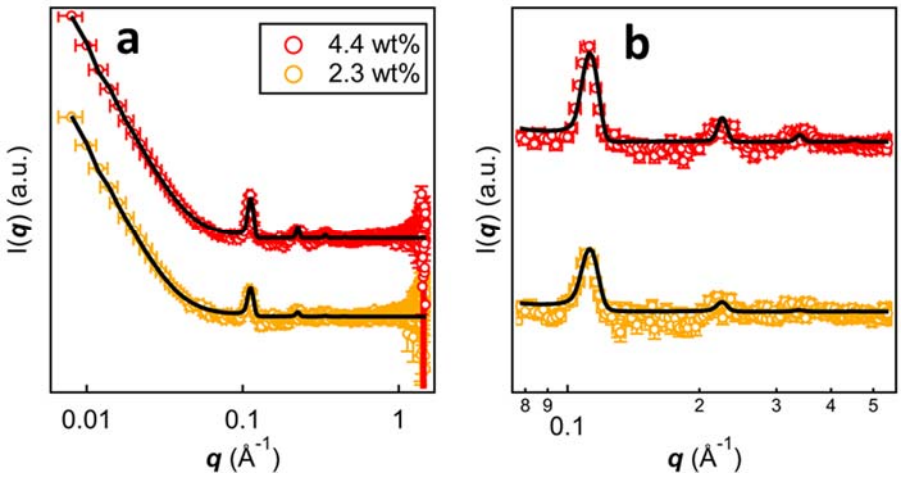

Figure S4 (**a**) Fitted SANS data for 4.4 wt% (red circles) and 2.3 wt% (orange circles) SDS in glycerol at 25 °C using the lamellar paracrystal stack model, with the Bragg peaks enlarged (**b**).

Table S12 A summary of the fitting parameters for 4.4 and 2.3 wt% SDS in glycerol, fitted to the lamellar paracrystal stack model: SDS bilayer thickness t_L, number of layers in the stack n_{Layers}, d-spacing, polydispersity of the d-spacing σ_d, scattering length density of SDS ρ_{SDS}, scattering length density of glycerol ρ_{Gly}, polydispersity of the SDS bilayer thickness σ_t, polydispersity of the d-Spacing thickness $\sigma_{d\text{-Spacing}}$, and chi squared value χ^2.

Parameter	4.4 wt%	2.3 wt%
Scale	0.613	0.225
Background (cm^{-1})	0.122	0.087
t_L (Å)	48.1	49.3
n_{layers}	21.0	21.4
d-Spacing (Å)	55.6	55.6
ρ_{SDS} (10^{-6} Å^{-2})	0.395	0.395
ρ_{Gly} (10^{-6} Å^{-2})	7.20	7.20
σ_t	0.01	0.04
$\sigma_{d\text{-Spacing}}$	0.00	0.10
χ^2	2.61	1.75

S4. Model refinement for the SANS data for the SDS-in-glycerol gel at 70 °C

The raw SANS profile of the gel at higher temperature indicated the presence of a micellar aggregate, the morphology of which was unknown, and thus, a variety of morphologies were tested (**Figure S5**). The fitted parameters are shown in **Table S13** - **Table S16**. The initial increase in the intensity indicated the presence of a structure factor, S(***q***), where the micelles were interacting with each other. The S(***q***) generally used in the fitting was a Hayter-MSA S(***q***), often used to describe ionic micelles in aqueous solutions, and was deemed appropriate here, despite being a mean sphere approximation.

From the initial primitive fitting analysis, the cylindrical F(***q***) and the ellipsoidal F(***q***) had the best fit from both the physical appearance and the χ^2 values. These two models were then used for further analysis, to determine the morphology with the best fit to the SANS profile.

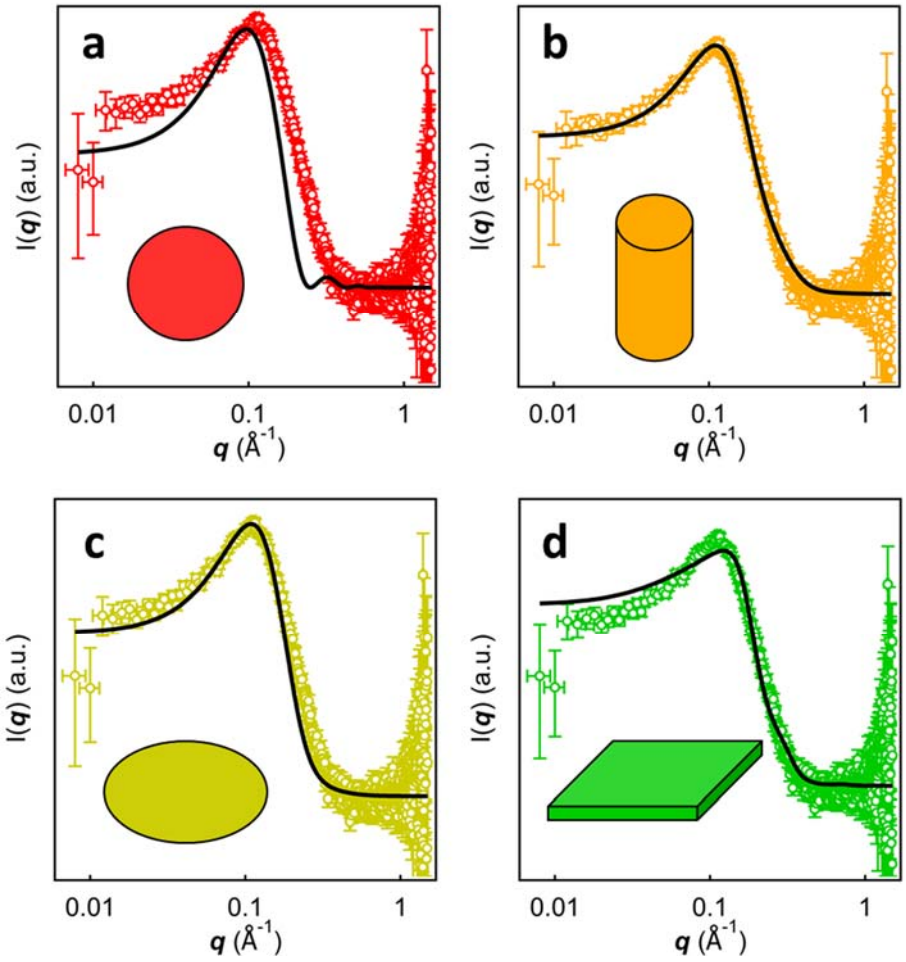

Figure S5 Fitted SANS data for 4.4 wt% SDS in glycerol at 70 °C using a Hayter-MSA S(***q***) and: (**a**) a spherical F(***q***); (**b**) a cylindrical F(***q***); (**c**) an ellipsoidal F(***q***); and (**d**) a parallepiped F(***q***). The appropriate morphology is shown as an **inset**.

Table S13 A summary of the fitting parameters for 4.4 wt% SDS in glycerol at 70 °C using a spherical F(***q***) and a Hayter-MSA S(***q***): scattering length density of SDS ρ_{SDS}, scattering length density of glycerol ρ_{Gly}, radius r, volume fraction φ, charge, temperature T, concentration of salt c_{salt}, dielectric constant ε, polydispersity of the radius σ_r, and chi squared value χ^2.

Parameter	Spherical F(q) with Hayter-MSA S(q)
Scale	0.12
Background (cm^{-1})	0.145
ρ_{SDS} (10^{-6} Å^{-2})	0.395
ρ_{Gly} (10^{-6} Å^{-2})	7.20
r (Å)	18.0
φ	0.10
Charge (e)	5.00
T (K)	343.0
c_{salt} (M)	0.00
ε	42.5
σ_r	0.00
χ^2	17.2

Table S14 A summary of the fitting parameters for 4.4 wt% SDS in glycerol at 70 °C using a cylindrical F(***q***) and a Hayter-MSA S(***q***): scattering length density of SDS ρ_{SDS}, scattering length density of glycerol ρ_{Gly}, radius r, length l, volume fraction φ, charge, temperature T, concentration of salt c_{salt}, dielectric constant ε, polydispersity of the radius σ_r, polydispersity of the length σ_l, and chi squared value χ^2.

Parameter	Cylindrical F(q) with Hayter-MSA S(q)
Scale	0.35
Background (cm^{-1})	0.145
ρ_{SDS} (10^{-6} Å^{-2})	0.395
ρ_{Gly} (10^{-6} Å^{-2})	7.20
r (Å)	17.0

l (Å)	10.0
φ	0.10
Charge (e)	5.00
T (K)	343.0
c_{salt} (M)	0.00
ε	42.5
σ_r	0.22
σ_l	0.24
χ^2	1.49

Table S15 A summary of the fitting parameters for 4.4 wt% SDS in glycerol at 70 °C using an ellipsoidal F($\boldsymbol{q}$) and a Hayter-MSA S($\boldsymbol{q}$): scattering length density of SDS ρ_{SDS}, scattering length density of glycerol ρ_{Gly}, polar radius r_{pol}, equatorial radius r_{eq}, volume fraction φ, charge, temperature T, concentration of salt c_{salt}, dielectric constant ε, polydispersity of the polar radius $\sigma_{r\text{-}pol}$, polydispersity of the equatorial radius $\sigma_{r\text{-}eq}$, and chi squared value χ^2.

Parameter	Ellipsoidal F(q) with Hayter-MSA S(q)
Scale	0.23
Background (cm^{-1})	0.145
ρ_{SDS} (10^{-6} Å^{-2})	0.395
ρ_{Gly} (10^{-6} Å^{-2})	7.20
r_{pol} (Å)	10.0
r_{eq} (Å)	18.0
φ	0.10
Charge (e)	5.00
T (K)	343.0
c_{salt} (M)	0.00
ε	42.5
$\sigma_{r\text{-}pol}$	0.20
$\sigma_{r\text{-}eq}$	0.20

χ^2	4.44

Table S16 A summary of the fitting parameters for 4.4 wt% SDS in glycerol at 70 °C using a parallepiped F(***q***) and a Hayter-MSA S(***q***): scattering length density of SDS ρ_{SDS}, scattering length density of glycerol ρ_{Gly}, length l_a, width l_b,, depth l_c, volume fraction φ, charge, temperature T, concentration of salt c_{salt}, dielectric constant ε, and chi squared value χ^2.

Parameter	Parallepiped F(*q*) with Hayter-MSA S(*q*)
Scale	0.17
Background (cm^{-1})	0.145
ρ_{SDS} (10^{-6} Å^{-2})	0.395
ρ_{Gly} (10^{-6} Å^{-2})	7.20
l_a (Å)	12.6
l_b (Å)	32.1
l_c (Å)	37.9
φ	0.20
Charge (e)	1.66
T (K)	343.0
c_{salt} (M)	0.00
ε	42.5
χ^2	2.06

Further refinement of the SANS data using the two models showed that the two models fitted well to the raw SANS profile (**Figure S6**), with the fitted parameters summarised in **Table S17** and **Table S18**. However, the fitting observed for the ellipsoidal model was based on parameters that were not physically feasible in some cases, such as the volume fraction, φ, ~ 0.002 or the concentration of salt, c_{salt}, ~ 0.1 M. Therefore, the cylindrical model was deemed more physically feasible and chosen as the appropriate model for the SANS profile.

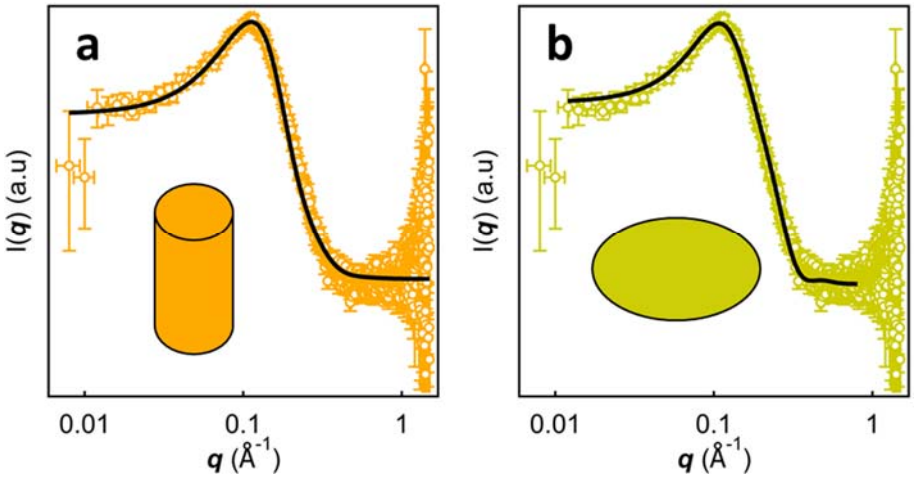

Figure S6 Further refined fitted SANS data for 4.4 wt% SDS in glycerol at 70 °C using a Hayter-MSA S(***q***) and: (**a**) a cylindrical F(***q***); and (**b**) an ellipsoidal F(***q***). The appropriate morphology is shown as an **inset**.

Table S17 A summary of the further refined fitting parameters for 4.4 wt% SDS in glycerol at 70 °C using a cylindrical F(***q***) and a Hayter-MSA S(***q***): scattering length density of SDS ρ_{SDS}, scattering length density of glycerol ρ_{Gly}, radius r, length l, volume fraction φ, charge, temperature T, concentration of salt c_{salt}, dielectric constant ε, polydispersity of the radius σ_r, polydispersity of the length σ_l, and chi squared value χ^2.

Parameter	Cylindrical F(*q*) with Hayter-MSA S(*q*)
Scale	0.26
Background (cm^{-1})	0.145
ρ_{SDS} (10^{-6} Å^{-2})	0.395
ρ_{Gly} (10^{-6} Å^{-2})	7.20
r (Å)	17.0
l (Å)	12.0
φ	0.12
Charge (e)	4.94
T (K)	343.0
c_{salt} (M)	0.00
ε	42.5
σ_r	0.23

σ_I	0.23
χ^2	1.39

Table S18 A summary of the further refined fitting parameters for 4.4 wt% SDS in glycerol at 70 °C using an ellipsoidal F(***q***) and a Hayter-MSA S(***q***): scattering length density of SDS ρ_{SDS}, scattering length density of glycerol ρ_{Gly}, polar radius r_{pol}, equatorial radius r_{eq}, volume fraction φ, charge, temperature T, concentration of salt c_{salt}, dielectric constant ε, polydispersity of the polar radius $\sigma_{r\text{-}pol}$, polydispersity of the equatorial radius $\sigma_{r\text{-}eq}$, and chi squared value χ^2.

Parameter	Ellipsoidal F(*q*) with Hayter-MSA S(*q*)
Scale	1.6
Background (cm^{-1})	0.14
ρ_{SDS} (10^{-6} Å^{-2})	0.395
ρ_{Gly} (10^{-6} Å^{-2})	7.20
r_{pol} (Å)	11.4
r_{eq} (Å)	13.2
φ	0.002
Charge (e)	30.0
T (K)	343.0
c_{salt} (M)	0.125
ε	42.5
$\sigma_{r\text{-}pol}$	0.20
$\sigma_{r\text{-}eq}$	0.10
χ^2	1.32

S5. Fitted SANS data for the SDS-in-glycerol gel at 70 °C

Figure S7 shows the fitted SANS profiles for the SDS-in-glycerol gel at 70 °C, for the SDS concentrations measured, fitted to a cylindrical F(***q***) combined with a Hayter-MSA S(***q***). The model is shown to be appropriate for the concentrations measured. The values of the fitted

parameters remained constant between the two concentrations measured, suggesting that the morphology did not change.

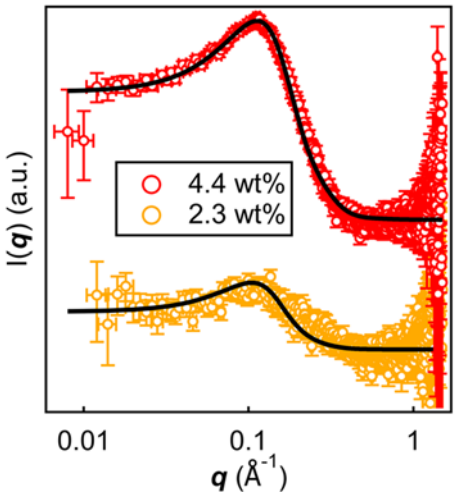

Figure S7 (**a**) Fitted SANS data for 4.4 wt% (red circles) and 2.3 wt% (orange circles) SDS in glycerol at 70 °C using a cylindrical F(***q***) combined with a Hayter-MSA S(***q***).

Table S19 A summary of the fitting parameters for 4.4 and 2.3 wt% SDS in glycerol at 70 °C, fitted to a cylindrical F(***q***) combined with a Hayter-MSA S(***q***): scattering length density of SDS ρ_{SDS}, scattering length density of glycerol ρ_{Gly}, radius r, length l, volume fraction φ, charge, temperature T, concentration of salt c_{salt}, dielectric constant ε, polydispersity of the radius σ_r, polydispersity of the length σ_l, and chi squared value χ^2.

Parameter	4.4 wt%	2.3 wt%
Scale	0.26	0.030
Background (cm^{-1})	0.145	0.0958
ρ_{SDS} (10^{-6} Å^{-2})	0.395	0.395
ρ_{Gly} (10^{-6} Å^{-2})	7.20	7.20
r (Å)	17.0	17.0
l (Å)	12.0	12.0
φ	0.12	0.11
Charge (e)	4.94	4.94
T (K)	343.0	343.0
c_{salt} (M)	0.00	0.00
ε	42.5	42.5

σ_r	0.23	0.30
σ_l	0.23	0.30
χ^2	1.39	1.35

S6. Fitted SANS data for SDS in glycerol for all temperatures

Figure S8 shows the fitted data for 4.4 wt % SDS in glycerol at all temperature measured, showing fits to the low temperature data (to a lamellar stack paracrystal model) and fits to the high temperature data (to a cylindrical F(***q***) and a Hayter MSA S(***q***)). **Figure S9** shows the fitted data for 2.3 wt % SDS in glycerol at all temperature measured, showing fits to the low temperature data (to a lamellar stack paracrystal model) and fits to the high temperature data (to a cylindrical F(***q***) and a Hayter MSA S(***q***)).

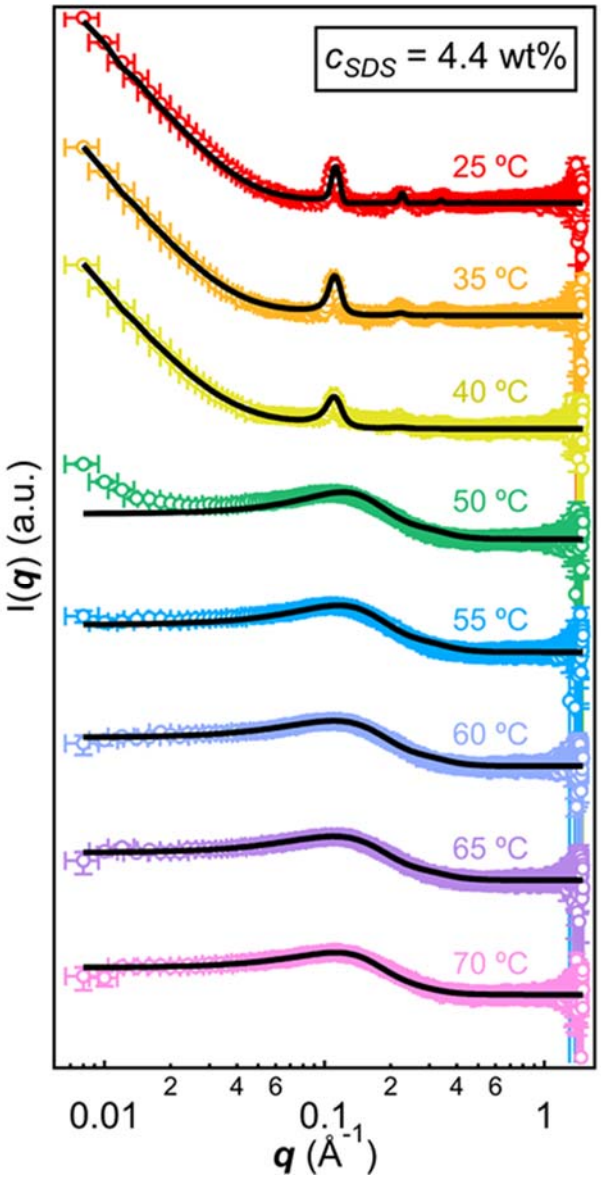

Figure S8 SANS profiles for 4.4 wt% (~14.7 CMC) *h*-SDS in *d*-glycerol at different temperatures, showing the transition between the micellar solution to the lamellar phase at a critical gelation temperature CGT ~ 40 – 50 °C. This figure includes the fits, at lower temperatures a lamellar stack paracrystal model, and at higher temperatures a cylindrical F(***q***) and a Hayter MSA S(***q***).

Table S20 A summary of the fitting parameters for 4.4 wt% SDS in glycerol at 25, 35, and 40 °C, fitted to the lamellar paracrystal stack model: SDS bilayer thickness t_L, number of layers in the stack n_{Layers}, *d*-spacing, polydispersity of the *d*-spacing σ_d, scattering length density of SDS ρ_{SDS}, scattering length density of glycerol ρ_{Gly}, polydispersity of the SDS bilayer thickness σ_t, polydispersity of the d-Spacing thickness $\sigma_{d\text{-}Spacing}$, and chi squared value χ^2.

Parameter	25 °C	35 °C	40 °C
Scale	0.613	0.343	0.299

Background (cm^{-1})	0.122	0.121	0.125
t_L (Å)	48.1	54.5	52.4
n_{layers}	21.0	22.3	22.1
d-Spacing (Å)	55.6	56.0	56.0
ρ_{SDS} (10^{-6} Å^{-2})	0.395	0.395	0.395
ρ_{Gly} (10^{-6} Å^{-2})	7.20	7.20	7.20
σ_t	0.01	0.09	0.13
$\sigma_{d\text{-}Spacing}$	0.00	0.10	0.32
χ^2	2.61	3.86	3.33

Table S21 A summary of the fitting parameters for 4.4 wt% SDS in glycerol at 50, 55, 60, 65, and 70 °C, fitted to a cylindrical F(***q***) combined with a Hayter-MSA S(***q***): scattering length density of SDS ρ_{SDS}, scattering length density of glycerol ρ_{Gly}, radius r, length l, volume fraction φ, charge, temperature T, concentration of salt c_{salt}, dielectric constant ε, polydispersity of the radius σ_r, polydispersity of the length σ_l, and chi squared value χ^2.

Parameter	50 °C	55 °C	60 °C	65 °C	70 °C
Scale	0.45	0.45	0.42	0.39	0.26
Background (cm^{-1})	0.145	0.145	0.145	0.145	0.145
ρ_{SDS} (10^{-6} Å^{-2})	0.395	0.395	0.395	0.395	0.395
ρ_{Gly} (10^{-6} Å^{-2})	7.20	7.20	7.20	7.20	7.20
r (Å)	17.0	17.0	17.0	17.0	17.0
l (Å)	10.1	10.0	10.1	10.1	12.0
φ	0.10	0.10	0.10	0.10	0.12
Charge (e)	6.00	6.00	4.00	4.00	4.94
T (K)	323.0	328.0	333.0	338.0	343.0
c_{salt} (M)	0.00	0.00	0.00	0.00	0.00
ε	42.5	42.5	42.5	42.5	42.5
σ_r	0.10	0.10	0.10	0.10	0.23
σ_l	0.10	0.10	0.10	0.10	0.23

χ^2	2.29	5.87	2.51	2.01	1.39

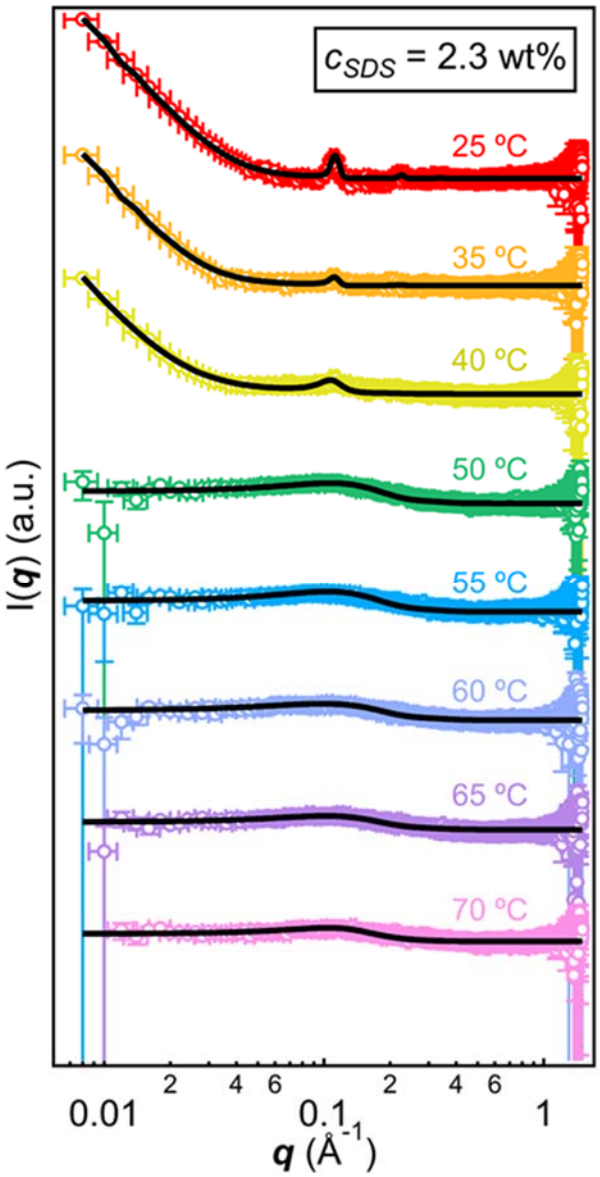

Figure S9 SANS profiles for 2.3 wt% (~7.68 CMC) *h*-SDS in *d*-glycerol at different temperatures, showing the transition between the micellar solution to the lamellar phase at a critical gelation temperature CGT ~ 40 – 50 °C. This figure includes the fits, at lower temperatures a lamellar stack paracrystal model, and at higher temperatures a cylindrical F(***q***) and a Hayter MSA S(***q***).

Table S22 A summary of the fitting parameters for 2.3 wt% SDS in glycerol at 25, 35, and 40 °C, fitted to the lamellar paracrystal stack model: SDS bilayer thickness t_L, number of layers in the stack n_{Layers}, *d*-spacing, polydispersity of the *d*-spacing σ_d, scattering length density of SDS ρ_{SDS},

scattering length density of glycerol ρ_{Gly}, polydispersity of the SDS bilayer thickness σ_t, polydispersity of the d-Spacing thickness $\sigma_{d\text{-}Spacing}$, and chi squared value χ^2.

Parameter	25 °C	35 °C	40 °C
Scale	0.225	0.074	0.044
Background (cm^{-1})	0.087	0.094	0.098
t_L (Å)	49.3	46.5	36.8
n_{layers}	21.4	21.2	25.1
d-Spacing (Å)	55.6	55.4	56.0
ρ_{SDS} (10^{-6} Å^{-2})	0.395	0.395	0.395
ρ_{Gly} (10^{-6} Å^{-2})	7.20	7.20	7.20
σ_t	0.04	0.09	0.20
$\sigma_{d\text{-}Spacing}$	0.10	0.00	0.50
χ^2	1.75	1.39	1.72

Table S23 A summary of the fitting parameters for 2.3 wt% SDS in glycerol at 50, 55, 60, 65, and 70 °C, fitted to a cylindrical F($\boldsymbol{q}$) combined with a Hayter-MSA S($\boldsymbol{q}$): scattering length density of SDS ρ_{SDS}, scattering length density of glycerol ρ_{Gly}, radius r, length l, volume fraction φ, charge, temperature T, concentration of salt c_{salt}, dielectric constant ε, polydispersity of the radius σ_r, polydispersity of the length σ_l, and chi squared value χ^2.

Parameter	50 °C	55 °C	60 °C	65 °C	70 °C
Scale	0.061	0.061	0.059	0.045	0.030
Background (cm^{-1})	0.098	0.098	0.10	0.10	0.096
ρ_{SDS} (10^{-6} Å^{-2})	0.395	0.395	0.395	0.395	0.395
ρ_{Gly} (10^{-6} Å^{-2})	7.20	7.20	7.20	7.20	7.20
r (Å)	16.9	16.9	16.9	16.9	17.0
l (Å)	11.8	11.8	10.0	10.0	12.0
φ	0.11	0.10	0.098	0.10	0.11
Charge (e)	3.44	3.44	2.45	3.00	4.94

T (K)	323.0	328.0	333.0	338.0	343.0
c_{salt} (M)	0.00	0.00	0.00	0.00	0.00
ε	42.5	42.5	42.5	42.5	42.5
σ_r	0.10	0.10	0.10	0.10	0.30
σ_l	0.10	0.10	0.10	0.10	0.30
χ^2	1.34	1.73	1.26	1.52	1.35

S7. Fitted SANS data for SDS in D_2O at 25 °C

h-SDS in D_2O was measured as a control to compare against the SDS in glycerol scattering profile, and these measurements were carried out at 25 °C only. The fitting analysis carried out here was consistent with the literature that show the morphology of SDS micelles to be spherical or ellipsoidal in shape. The fitted data is shown in **Figure S10**, and the fitting parameters are summarised in **Table S24**.

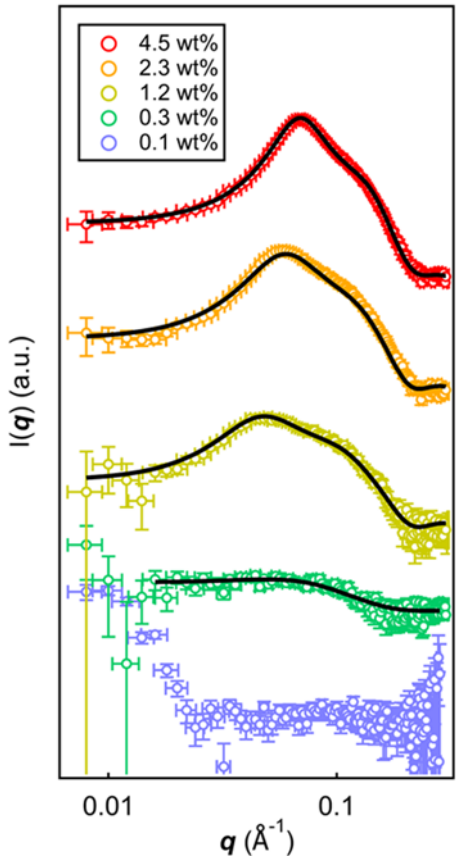

Figure S10 Fitted SANS profiles for various concentrations of SDS in D_2O, a control for the SDS-in-glycerol gel at 25 °C. The model chosen for the fitted data was a core-shell-sphere F(***q***) and a Hayter-MSA S(***q***).

Table S24 A summary of the fitting parameters for 4.5, 2.3, 1.2, and 0.3 wt% SDS in D_2O at 25 °C, fitted to a core-shell-sphere F(***q***) combined with a Hayter-MSA S(***q***): scattering length density of the SDS headgroup ρ_{HG}, scattering length density of the SDS tail ρ_{tail}, scattering length density of glycerol ρ_{Gly}, radius r, core thickness t, volume fraction φ, charge, temperature T, salt concentration c_{salt}, dielectric constant ε, polydispersity of the radius σ_r, polydispersity of the core thickness σ_t, and chi squared value χ^2.

Parameter	4.5 wt%	2.3 wt%	1.2 wt%	0.3 wt%
Scale	1.22	0.79	0.36	0.05
Background (cm^{-1})	0.094	0.077	0.034	0.048
ρ_{HG} (10^{-6} Å^{-2})	-0.29	-0.29	-0.25	-0.35
ρ_{tail} (10^{-6} Å^{-2})	4.95	4.95	5.70	5.00
ρ_{Gly} (10^{-6} Å^{-2})	6.64	6.64	6.71	6.85
r (Å)	18.0	19.0	19.3	17.4

t (Å)	2.0	2.0	2.1	2.0
φ	0.0311	0.0215	0.0100	0.0100
Charge (e)	40.2	26.0	24.8	35.0
T (K)	298.0	298.6	294.0	301.0
c_{salt} (M)	0.00	0.00	0.00	0.09
ε	80.1	80.1	80.1	80.1
σ_r	0.15	0.09	0.00	0.20
σ_t	0.10	0.10	0.00	0.09
χ^2	1.18	1.16	0.97	0.76

S8. Scaling of SANS curves to observe aggregate dimensionality

The SANS curves in the main text are reproduced below with the y-axis scaling shown.

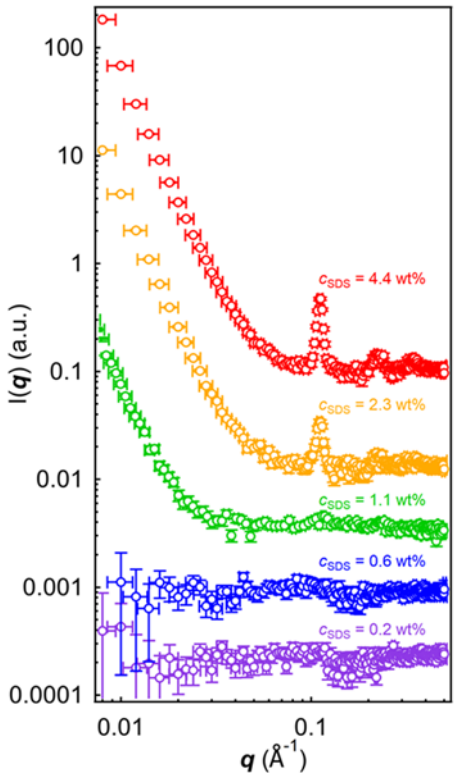

Figure S11 SANS profiles for *h*-SDS in *d*-glycerol at various surfactant concentrations c_{SDS} at room temperature. The profiles are offset on the vertical scale for clarity. This is reproduced from **Figure 9** in the main text reproduced with scaling on the vertical scale shown.

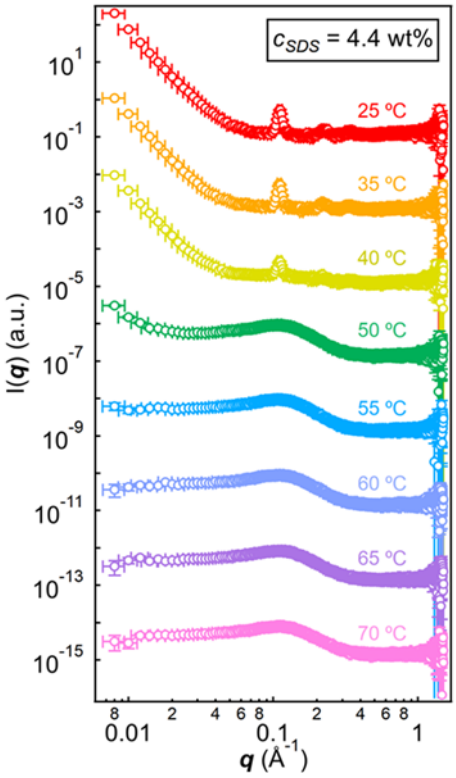

Figure S12 SANS profiles for 4.4 wt% (~14.7 CMC) *h*-SDS in *d*-glycerol at different temperatures, showing the transition between the micellar solution to the lamellar phase at a critical gelation temperature CGT ~ 40 – 50 °C. The profiles are offset on the vertical scale for clarity. This is reproduced from **Figure 10** in the main text reproduced with scaling on the vertical scale shown.